Coordinated Direct and Relay Transmission With NOMA and Network Coding in Nakagami-m Fading Channels

***Abstract*—Although the use of coordinated direct and relay transmission (CDRT) in non-orthogonal multiple access (NOMA) can extend the coverage, its duplicated transmission reduces the spectrum efficiency (SE) of NOMA. To improve the SE, we propose a spectrum-efficient scheme for NOMA-based CDRT over Nakagami-m fading channels. In this scheme, the base station (BS) connects with a cell-center user (CCU) directly while communicating with a cell-edge user (CEU) via a relay and the CCU. Then, the relay and the CCU use network coding to process and retransmit the signals sent by the BS first and the CEU later. Finally, the BS and the relay simultaneously broadcast downlink signals. We derive the closed-form expressions for the average SE, the user fairness index and the energy efficiency (EE) as well as the asymptotic average SE using both perfect and imperfect successive interference cancellation (SIC). Simulations verify the correctness of our theoretical analysis and the superiority of the proposed scheme in SE and EE.**

***Index Terms*—Coordinated direct and relay transmission, Nakagami-m fading, non-orthogonal multiple access (NOMA), spectrum efficiency, successive interference cancellation (SIC).**

I. Introduction

FUTURE wireless networks need higher spectrum efficiency (SE), lower handover latency and larger coverage to enable massive machine communications from Internet of Things (IoT) related applications [1], [2]. To meet these requirements, non-orthogonal multiple access (NOMA) has been investigated as a promising candidate [3], [4]. Compared with orthogonal multiple access (OMA), NOMA exploits the power and channel differences to enable different users to simultaneously share the same radio resource, such as communication time, frequency, and code. To enable NOMA, superposition coding and successive interference cancellation (SIC) are performed at the transmitter and the receiver, respectively [5]. Since NOMA can provide higher SE and massive connectivity, several wireless technologies have been combined with NOMA to further unlock their great potentials, including energy harvesting [6]–[8], massive multi-input and multi-output (MIMO) [9], millimeter wave (mmWave) communications [10], cooperative relaying [11], physical layer security [12]–[14], orthogonal time frequency space (OTFS) modulation [15] and intelligent reflecting surface (IRS) [16].

In particular, the integration of cooperative relaying and NOMA has attracted significant attention because of its ability to improve the SE and expand the coverage [17]–[21]. Cooperative NOMA (CNOMA) was first introduced by Ding *et al.* in [17] to improve the system reliability, where stronger users act as relays to help weaker users. In [18], Men *et al.* studied the outage performance and the ergodic sum rate for the NOMA-based AF relaying networks over Nakagami-m fading channels. Lv *et al.* proposed a NOMA-based cooperative transmission scheme in [19] to achieve better spectrum utilization for spectrum-sharing cognitive radio networks. In [20], Mei *et al.* proposed a novel uplink cooperative NOMA to mitigate the severe uplink interference for cellular-connected unmanned aerial vehicle (UAV) networks. An optimal power allocation was characterized by Zhang *et al.* in [21] to minimize the outage probability and maximize the minimum achievable rate for CNOMA with full-duplex relaying. However, achieving superior SE and wider coverage remains a great challenge in CNOMA networks due to poor channel condition between the base station (BS) and the cell-edge user (CEU).

Coordinated direct and relay transmission (CDRT), consisting of direct and relayed transmissions, is evolved from the two-way relay system adopting the analog network coding [22]. Since CDRT can provide a significant performance gain, it has been combined with NOMA to further improve the SE and coverage of CNOMA [23]. In [23], Kim *et al.* first investigated NOMA-based CDRT in a downlink scenario by exploiting the side information of the CEU to achieve superior SE. Based on this work, some research efforts have been dedicated to analyzing the performance of NOMA-based CDRT systems [24]–[29]. In [24], a downlink NOMA-based CDRT system using the full-duplex relay was investigated by Zhong *et al.* in terms of outage performance and ergodic sum capacity (ESC). In [25], Aswathi *et al.* considered full/half duplex relaying for downlink NOMA-based CDRT

xuyao_hit@sina.com; libo1983@hit.edu.cn; gwang51@hit.edu.cn).

xianbin.wang@uwo.ca).

with imperfect SIC. In [26], Liu *et al.* proposed a selective DF scheme for NOMA-based CDRT to improve the outage performance of far users. Then, the capacity of uplink NOMA-based CDRT was analyzed by Kader *et al.* in [27]. A dynamic scheme was proposed by Xu *et al.* in [28] to enhance the system reliability of downlink NOMA-based CDRT, and a relay selection strategy was studied by Yang *et al.* in [29] to improve the outage performance of the CEU. The capacity scaling for a new device-to-device (D2D) assisted CNOMA scheme was analyzed by Kim *et al.* in [30], and Zou *et al.* used the similar frame to study the application of D2D communication in downlink NOMA-based CDRT system [31]. Moreover, a satellite-aided CDRT system using NOMA was proposed by Li *et al.* in [32] to support robust communication for the specific environment. Cao *et al.* analyzed the secrecy performance of NOMA-based CDRT with multi-antenna full-duplex relay in [33]. In addition, Guo *et al.* investigated the application of SWIPT to downlink NOMA-based CDRT in [34] to compensate for the energy loss of relay. On the other hand, the resource allocation problems have also been studied for NOMA-based CDRT systems [35], [36]. Particularly, Chen *et al.* addressed the resource allocation problems for downlink NOMA-based CDRT in [35]. In [36], Li *et al.* adopted the Hungarian algorithm and the Lagrange dual method to design an optimal solution for maximizing the throughput of NOMA-based CDRT systems.

In NOMA-based CDRT systems, the BS needs relay assistance to communicate with the CEU due to the deep fading. However, the duplicated transmissions at the relay or the cell-center user (CCU) may prevent NOMA from achieving higher SE. In addition, the mutual interference between the relay and the CCU always exists in both uplink and downlink transmissions according to NOMA, which can decrease the SE. However, most existing works only focus on the reliability improvement and resource allocation with Rayleigh fading channels. Motivated by the above observations, we aim to provide superior SE for NOMA-based CDRT systems via jointly designing the uplink and downlink transmissions. The main contributions of this paper are summarized as follows.

- In NOMA-based CDRT, both the duplicated transmission and the mutual interference may reduce the SE superiority of NOMA. To address this problem, we propose a spectrum-efficient scheme to achieve better SE for NOMA-based CDRT systems. In this scheme, the CEU communicates with a base station (BS) with the help of a relay, and the CCU can directly communicate with the BS. Specifically, the uplink and downlink transmissions are jointly designed via network coding to save time resource and further improve the SE.
- We investigate the proposed scheme over Nakagami-m fading channel with both perfect and imperfect SIC. First, we derive the closed-form expressions of the ESC for the uplink and downlink transmissions of the proposed scheme, respectively. To measure the performance from an overall perspective, we further study the average SE of the proposed scheme. Then, the asymptotic expressions for the average SE of the proposed scheme are also attained.

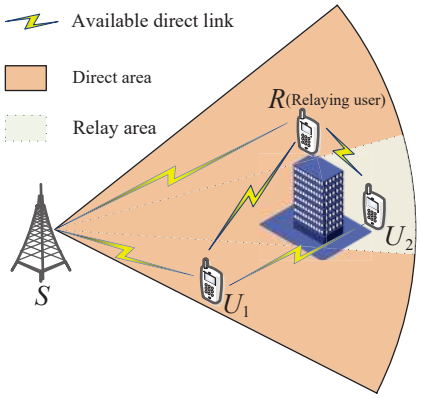

Fig. 1. System model of NCDRT with a BS, a DF relaying user, a cell-center user and a cell-edge user.

- To obtain more practical insights, we characterize the user fairness of the proposed scheme by using Jain's fairness index. Next, the impact of the fading parameter on the average SE is also simulated and discussed.
- To verify the effectiveness of the proposed scheme, we derive the closed-form expressions of the energy efficiency gains over the other three benchmarks, including a conventional NOMA-based CDRT scheme and two OMA schemes.

The rest of the paper is organized as follows. In Section II, the system model of NOMA-based CDRT is presented. Section III provides the details of the proposed scheme. In Section IV, the closed-form expressions for average SE, user fairness index and EE gain are derived. Simulation results are given in Section V, and we conclude this work in Section VI.

Notations: In this paper, the probability density function (PDF) and the cumulative distribution function (CDF) of a random variable Z are denoted by $f_Z(\cdot)$ and $F_Z(\cdot)$, respectively; $\mathbb{E}(\cdot)$ denotes the expectation operator; $C_A = C_B(a \Rightarrow b)$ denotes the operation to obtain C_A after replacing all a in C_B with b; "$\rightarrow$" means "be proportional to".

II. System Model

A. System Configuration

As shown in Fig. 1, we consider a single-cell NOMA-based CDRT (NCDRT) system, which consists of one BS (S), one CCU (U_1), one CEU (U_2) and one decode-and-forward (DF) relaying user (R). Similar to [30] and [31], a CCU close to U_2 can be selected as the relaying user, and the system model can be considered as a simple connected D2D-assisted cellular model. Due to the significant shadowing, the direct link between the BS and U_2 does not exist [23]. Thus, the BS can directly communicate with U_1 and R, while it needs relay assistance from either R or U_1 to communicate with U_2. Each node has a single antenna and operates in half-duplex mode. Assume that all channel links experience independent and identically distributed Nakagami-m fading channels and additive white Gaussian noise (AWGN) with zero mean and variance N_0. Since this system performs in a time-division duplex (TDD) model, the reciprocity between downlink and

uplink is assumed in this paper [37], [38]. Hereafter, let subscripts s, r, 1 and 2 represent S, R, U_1 and U_2, respectively. The distance, channel power and channel coefficient between $\tilde{x}$ and $\tilde{y}$ are denoted by $d_{\tilde{x}\tilde{y}}$, $\lambda_{\tilde{x}\tilde{y}}$ and $h_{\tilde{x}\tilde{y}}$ with fading parameter $m_{\tilde{x}\tilde{y}}$ and $\mathbb{E}\{|h_{\tilde{x}\tilde{y}}|^2\} = \Omega_{\tilde{x}\tilde{y}}$, respectively, where $\tilde{x}, \tilde{y} \in \{s, r, 1, 2\}$, $\tilde{x} \neq \tilde{y}$. In this paper, we assume that $\Omega_{s1} > \max\{\Omega_{sr}, \Omega_{r1}\}$ and $\Omega_{r2} > \max\{\Omega_{12}, \Omega_{r1}\}$, which may not guarantee $|h_{s1}|^2 > \max\{|h_{sr}|^2, |h_{r1}|^2\}$ and $|h_{r2}|^2 > \max\{|h_{12}|^2, |h_{r1}|^2\}$. It is worth pointing out that the proposed scheme can be easily extended to other channel assumptions via NOMA.

B. Channel Model

In this paper, we consider Nakagami-m channel model, and assume that the m parameters are integers. Then, if the channel coefficient Z exhibits Nakagami-m distribution with an integer fading parameter m_z and $\mathbb{E}\{|Z|^2\} = \Omega_z$, the corresponding channel gain $|Z|^2$ follows Gamma distribution and its probability density function (PDF) and cumulative distribution function (CDF) can be expressed as

$$f_{|Z|^2}(z) = \frac{{m_z}^{m_z} z^{m_z-1}}{{\Omega_z}^{m_z}\Gamma(m_z)} \exp\left(-\frac{m_z z}{\Omega_z}\right), \quad (1)$$

$$F_{|Z|^2}(z) = 1 - \exp\left(-\frac{m_z z}{\Omega_z}\right) \sum_{b=0}^{m_z-1} \left(\frac{m_z z}{\Omega_z}\right)^b / b!, \quad (2)$$

where $\Gamma(\cdot)$ denotes the Gamma function. Note that when m_z takes positive integer values, the equation $\Gamma(m_z) = (m_z - 1)!$ always holds.

III. Spectrum-Efficient NCDRT Scheme

In the existing NOMA-based CDRT works, the uplink and downlink transmissions are always investigated separately, which may not fully utilize the high SE feature and prior information of NOMA. To address this problem, we try to jointly design the uplink and downlink transmissions via network coding. Thus, we propose a spectrum-efficient scheme, as illustrated in Fig. 2, which consists of four consecutive and equal phases (i.e., t_1, t_2, t_3, t_4).

A. First Phase (t_1)

In the first phase, the BS broadcasts $\sqrt{\alpha_1 P_s}x_1 + \sqrt{\alpha_2 P_s}x_2$ via downlink NOMA, where x_i is the data for U_i, $i \in \{1, 2\}$, P_s is the transmit power of BS, and α_i denotes the power allocation (PA) coefficient. Based on downlink NOMA, the conditions $\alpha_1 < \alpha_2$ and $\sum_{i=1}^{2} \alpha_i = 1$ should be satisfied due to $\Omega_{s1} > \Omega_{sr}$. The received signals at R and U_1 can be expressed as

$$y_r^{t_1} = h_{sr}(\sqrt{\alpha_1 P_s}x_1 + \sqrt{\alpha_2 P_s}x_2) + n_r^{t_1}, \quad (3)$$

$$y_1^{t_1} = h_{s1}(\sqrt{\alpha_1 P_s}x_1 + \sqrt{\alpha_2 P_s}x_2) + n_1^{t_1}, \quad (4)$$

where $n_{\tilde{x}}^{t_j} \sim \mathcal{CN}(0, N_0)$ denotes the AWGN at $\tilde{x}$ in t_j, $\tilde{x} \in \{s, r, 1, 2\}$ and $j \in \{1, 2, 3, 4\}$. The relay R can directly decode x_2 by treating x_1 as noise, while U_1 performs SIC to decode x_1 after removing x_2. Thus, the received signal-to-interference-plus-noise ratio (SINR) at R and U_1 can be written as

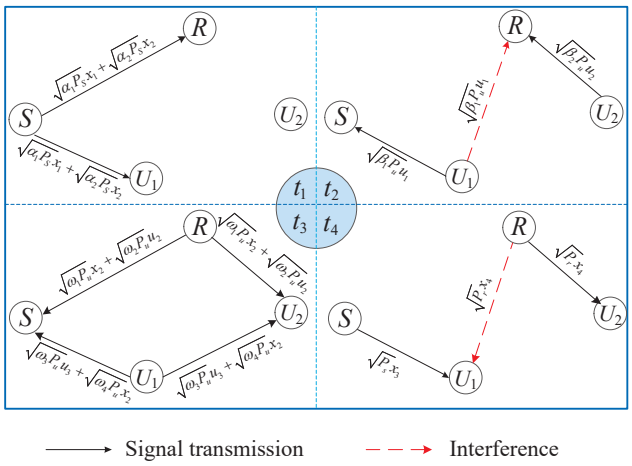

Fig. 2. An illustration of the proposed scheme for CDRT. The whole transmission process consists of four consecutive and equal phases.

$$\gamma_{r,x_2}^{t_1} = \frac{\lambda_{sr}\alpha_2\rho_s}{\lambda_{sr}\alpha_1\rho_s + 1}, \quad (5)$$

$$\gamma_{1,x_2}^{t_1} = \frac{\lambda_{s1}\alpha_2\rho_s}{\lambda_{s1}\alpha_1\rho_s + 1}, \quad (6)$$

$$\gamma_{1,x_1}^{t_1} = \frac{\lambda_{s1}\alpha_1\rho_s}{\dot{\lambda}_{s1}\alpha_2\rho_s + 1}, \quad (7)$$

where $\rho_s = \frac{P_s}{N_0}$ denotes the transmit signal-to-noise ratio (SNR), $\dot{\lambda}_{s1} = |\dot{h}_{s1}|^2$ and $\dot{h}_{s1}$ exhibits Nakagami-m fading with parameter m_{s1} and $\mathbb{E}\{\dot{\lambda}_{s1}\} = \vartheta_1\Omega_{s1}$. The ratio ϑ_1 ($0 \leq \vartheta_1 \leq 1$) denotes the residual interference level caused by imperfect SIC at U_1. Note that $\vartheta_1 = 0$ and $\vartheta_1 = 1$ represent the cases of perfect SIC and no SIC at U_1, respectively.

B. Second Phase (t_2)

According to uplink NOMA, U_1 and U_2 transmit $\sqrt{\beta_1 P_u}u_1$ and $\sqrt{\beta_2 P_u}u_2$ in t_2, respectively, where β_i is the PA coefficient, and P_u denotes the total uplink transmit power. Due to $\Omega_{r2} > \Omega_{r1}$, the PA coefficients should meet $\beta_1 < \beta_2$ and $\sum_{i=1}^{2} \beta_i = 1$ to perform uplink NOMA. The observations at S and R in t_2 can be expressed as

$$y_s^{t_2} = h_{s1}\sqrt{\beta_1 P_u}u_1 + n_s^{t_2}, \quad (8)$$

$$y_r^{t_2} = h_{r1}\sqrt{\beta_1 P_u}u_1 + h_{r2}\sqrt{\beta_2 P_u}u_2 + n_r^{t_2}. \quad (9)$$

Similarly, R tries to decode u_2 by treating u_1 as interference, while the BS can directly decode u_1. Thus, the corresponding received SINRs can be written as

$$\gamma_{s,u_1}^{t_2} = \lambda_{s1}\beta_1 a_1 \rho_s, \quad (10)$$

$$\gamma_{r,u_2}^{t_2} = \frac{\lambda_{r2}\beta_2 a_1 \rho_s}{\lambda_{r1}\beta_1 a_1 \rho_s + 1}, \quad (11)$$

where $a_1 = \frac{P_u}{P_s}$ denotes a scale factor.

C. Third Phase (t_3)

In the third phase, the proposed scheme utilizes network coding and prior information obtained by NOMA to jointly design the transmission process to improve the SE. Specifically, R transmits $\sqrt{\omega_1 P_u}x_2 + \sqrt{\omega_2 P_u}u_2$ after re-encoding the decoded x_2 and u_2. Simultaneously, U_1 tries to send the combination of the decoded x_2[1] and a new signal u_3, i.e., $\sqrt{\omega_3 P_u}u_3 + \sqrt{\omega_4 P_u}x_2$, for further enhancing the system SE, where u_3 is the uplink signal of U_1. The PA coefficient $\omega_j, j \in \{1,2,3,4\}$ satisfies $\sum_{j=1}^{4}\omega_j = 1$. To perform uplink NOMA at S, the PA coefficients satisfy $\omega_3 > \omega_2$ due to $\Omega_{s1} > \Omega_{sr}$. Besides, the conditions $\omega_4 > \omega_3$ and $\omega_1 \neq 0$ should be met to guarantee the EC of x_2 via diversity combining. The received signals at S and U_2 in t_3 can be expressed as

$$\begin{aligned} y_s^{t_3} =& h_{sr}(\sqrt{\omega_1 P_u}x_2 + \sqrt{\omega_2 P_u}u_2) \\ &+ h_{s1}(\sqrt{\omega_3 P_u}u_3 + \sqrt{\omega_4 P_u}x_2) + n_s^{t_3}, \end{aligned} \tag{12}$$

$$\begin{aligned} y_2^{t_3} =& h_{r2}(\sqrt{\omega_1 P_u}x_2 + \sqrt{\omega_2 P_u}u_2) \\ &+ h_{12}(\sqrt{\omega_3 P_u}u_3 + \sqrt{\omega_4 P_u}x_2) + n_2^{t_3}. \end{aligned} \tag{13}$$

Particularly, after estimating $h_{sr}\sqrt{\omega_1 P_u}$ and $h_{s1}\sqrt{\omega_4 P_u}$ [2], the BS can use the known signal x_2 to remove the interference $h_{sr}\sqrt{\omega_1 P_u}x_2 + h_{s1}\sqrt{\omega_4 P_u}x_2$ in (12) and decode u_3 and u_2 sequentially via SIC. Similarly, U_2 removes the interference $h_{r2}\sqrt{\omega_2 P_u}u_2$ by estimating $h_{r2}\sqrt{\omega_2 P_u}$. Meanwhile, U_2 uses the two copies of x_2 from R and U_1 to decode x_2 via selection combining (SC) or maximal-ratio combining (MRC) [39] and treating u_3 as noise. As a result, the side information of x_2 obtained by SIC at U_1 is fully used to improve the system performance. Based on the above analysis, the received SINRs at S and U_2 can be written as

$$\gamma_{s,u_3}^{t_3} = \frac{\lambda_{s1}\omega_3 a_1 \rho_s}{\lambda_{sr}\omega_2 a_1 \rho_s + 1}, \tag{14}$$

$$\gamma_{s,u_2}^{t_3} = \frac{\lambda_{sr}\omega_2 a_1 \rho_s}{\ddot{\lambda}_{s1}\omega_3 a_1 \rho_s + 1}, \tag{15}$$

$$\gamma_{2,x_2}^{t_3,\mathrm{SC}} = \max\left\{\lambda_{r2}\omega_1 a_1 \rho_s, \frac{\lambda_{12}\omega_4 a_1 \rho_s}{\lambda_{12}\omega_3 a_1 \rho_s + 1}\right\}, \tag{16}$$

$$\gamma_{2,x_2}^{t_3,\mathrm{MRC}} = \lambda_{r2}\omega_1 a_1 \rho_s + \frac{\lambda_{12}\omega_4 a_1 \rho_s}{\lambda_{12}\omega_3 a_1 \rho_s + 1}, \tag{17}$$

where $\ddot{\lambda}_{s1} = |\ddot{h}_{s1}|^2$ follows a Gamma distribution. Similar to ϑ_1, ϑ_2 denotes the interference level of imperfect SIC at S.

D. Fourth Phase (t_4)

Due to the short-distance feature of D2D link between the relaying user (i.e., R) and the CEU (i.e., U_2), a CCU close to U_2 can be selected as a relay to perform the proposed scheme [30], [31]. Thus, R is allowed to transmit its own signal to U_2, which can offload the traffic and further enhance the SE. Specifically, the BS and R simultaneously broadcast new signals x_3 and x_4 with powers P_s and P_r in t_4, respectively, where P_r denotes the transmit power of R. The signal x_3 is required by U_1 and x_4 is for U_2. Thus, the corresponding received SINRs at U_1 and U_2 are given as

$$\gamma_{1,x_3}^{t_4} = \frac{\lambda_{s1}\rho_s}{\lambda_{r1}a_2\rho_s + 1}, \tag{18}$$

$$\gamma_{2,x_4}^{t_4} = \lambda_{r2}a_2\rho_s, \tag{19}$$

where $a_2 = \frac{P_r}{P_s}$ is a scale factor.

To reduce system complexity for the practical implementation, we can extend the proposed scheme to a multi-user scenario (i.e., more than two users) straightforwardly by adopting user pairing and hybrid multiple access. Specifically, we can first divide the users in a single-cell into different groups via user pairing. Then, the proposed NCDRT scheme can be directly implemented within each group, while the conventional OMA (i.e., TDMA, CDMA and FDMA) is adopted to serve different user pairs [17], [41]. Similar to [23] and [27], we focus on the scheme design and performance analysis for NOMA-based CDRT systems in this work. Thus, the user pairing problem is beyond the scope of the paper.

IV. Performance Analysis

In this section, we derive the closed-form expressions of the ergodic capacity (EC), average SE, user fairness index, and energy efficiency (EE) for the proposed scheme with both perfect and imperfect SIC over Nakagami-m fading channels. Note that average SE is a key metric of system performance when the target rates vary with the channel conditions. To facilitate the analysis, we consider the unit time (i.e., 1s) and normalized bandwidth (i.e., 1Hz) in this paper as in [30]. Thus, the average SE can be straightforwardly obtained from the analysis of the EC. Let P, Q_1, Q_2, Q_3, Q_4, S_1, S_2 and U denote $\gamma_{1,x_1}^{t_1}$, $\gamma_{1,x_2}^{t_1}$, $\gamma_{r,x_2}^{t_1}$, $\gamma_{2,x_2}^{t_3,\mathrm{SC}}$, $\gamma_{2,x_2}^{t_3,\mathrm{MRC}}$, $\gamma_{r,u_2}^{t_2}$, $\gamma_{s,u_2}^{t_3}$ and $\gamma_{s,u_3}^{t_3}$, respectively.

A. Ergodic Capacities of Downlink Signals

When U_1 performs perfect SIC (i.e., $\vartheta_1 = 0$) in t_1, we can use (2) and (7) to obtain the CDF of P as

$$F_P(p) = 1 - \exp\left(-\frac{m_{s1}p}{\alpha_1\rho_s\Omega_{s1}}\right)\sum_{b=0}^{m_{s1}-1}\left(\frac{m_{s1}p}{\alpha_1\rho_s\Omega_{s1}}\right)^b/b!. \tag{20}$$

Using (20), the EC of x_1 is derived as

$$\begin{aligned} C_{x_1}^{p} =& \frac{1}{4}\int_0^\infty \log(1+P) f_P(p) dp \\ \overset{(a)}{=}& \frac{1}{4\ln 2}\sum_{b=0}^{m_{s1}-1}\left(\frac{m_{s1}}{\alpha_1\rho_s\Omega_{s1}}\right)^b/b! \\ &\times \int_0^\infty \frac{p^b}{1+p}\exp\left(-\frac{m_{s1}p}{\alpha_1\rho_s\Omega_{s1}}\right)dp \\ \overset{(b)}{=}& \frac{1}{4\ln 2}\sum_{b=0}^{m_{s1}-1}\left(\frac{m_{s1}}{\alpha_1\rho_s\Omega_{s1}}\right)^b/b! I_1\left(b, \frac{m_{s1}}{\alpha_1\rho_s\Omega_{s1}}, b_1\right). \end{aligned} \tag{21}$$

[1]Since U_2 will suffer the interference u_3 from U_1 in t_3, the cooperative link between U_1 and U_2 can further improve the EC of x_2 under the statistical channel state information.

[2]The BS can estimate all the uplink channel coefficients in t_3 by using the existing channel estimation schemes, such as channel estimation using designed preamble [40] and two-step channel estimation [38]. Since the proposed scheme is a TDD-based NOMA system, the BS can also use channel reciprocity to obtain the uplink channel coefficients based on downlink channel estimation [40].

In (21), (a) follows

$$\int_0^\infty \log_2(1+z) f_Z(z) dz = \frac{1}{\ln 2}\int_0^\infty \frac{1-F_Z(z)}{1+z} dz, \quad (22)$$

and (b) follows [42, eq.(3.353.5)] with

$$I_1(\varphi,\mu,\upsilon) \triangleq \int_0^\infty \frac{z^\varphi}{1+z}\exp(-\mu z)dz$$
$$= (-1)^{\varphi-1}e^{\mu}\mathrm{Ei}(-\mu) + \sum_{\upsilon=1}^{\varphi}(\upsilon-1)!(-1)^{\varphi-\upsilon}\mu^{-\upsilon}, \quad (23)$$

where $\mathrm{Ei}(\cdot)$ represents the exponential integral function. With imperfect SIC (i.e., $\vartheta_1 \neq 0$), we can rewrite (20) as

$$F_P(p) = \int_0^\infty F_{\lambda_{s1}}\left(\frac{(x\alpha_2\rho_s+1)p}{\alpha_1\rho_s}\right) f_{\dot{\lambda}_{s1}}(x)dx$$
$$\overset{(c)}{=} 1 - \Delta_{b,b_1}(p+A)^{-(b_1+m_{s1})}p^b \exp\left(-\frac{m_{s1}p}{\alpha_1\rho_s\Omega_{s1}}\right), \quad (24)$$

where $\Delta_{b,b_1} = \frac{{m_{s1}}^{m_{s1}}}{(\vartheta_1\Omega_{s1})^{m_{s1}}\Gamma(m_{s1})}\sum_{b=0}^{m_{s1}-1}\sum_{b_1=0}^{b}\binom{b}{b_1}{\rho_s}^{b_1-b}\times {\alpha_2}^{-m_{s1}}\frac{(b_1+m_{s1}-1)!}{b!}(\frac{m_{s1}}{\alpha_1\Omega_{s1}})^{b-b_1-m_{s1}}$, $A = \frac{\alpha_1}{\vartheta_1\alpha_2}$. The step (c) uses the binomial expansion $(\frac{(x\alpha_2\rho_s+1)p}{\alpha_1\rho_s})^b = \sum_{b_1=0}^{b}\binom{b}{b_1}(\frac{p}{\alpha_1})^b{\rho_s}^{b_1-b}(\alpha_2 x)^{b_1}$ and [42, eq.(3.351.3)]. Based on (22) and (24), the EC of x_1 with imperfect SIC is calculated as

$$C_{x_1} = \frac{\Delta_{b,b_1}}{4\ln 2}\int_0^\infty \frac{p^b\exp\left(-\frac{m_{s1}p}{\alpha_1\rho_s\Omega_{s1}}\right)}{(p+A)^{b_1+m_{s1}}(P+1)}dp$$
$$\overset{(d)}{=} \frac{\Delta_{b,b_1}}{4\ln 2}\Bigg\{\sum_{b_2=1}^{b_1+m_{s1}}-\left(\frac{1}{A-1}\right)^{b_2}$$
$$\times \underbrace{\int_0^\infty \frac{p^b}{(p+A)^{\bar{b}}}\exp\left(-\frac{m_{s1}p}{\alpha_1\rho_s\Omega_{s1}}\right)dp}_{\Theta_1} + \left(\frac{1}{A-1}\right)^{b_1+m_{s1}}$$
$$\times \underbrace{\int_0^\infty \frac{p^b}{p+1}\exp\left(-\frac{m_{s1}p}{\alpha_1\rho_s\Omega_{s1}}\right)dp}_{\Theta_2}\Bigg\}, \quad (25)$$

where $\bar{b} = b_1 + m_{s1} - b_2 + 1$, and (d) follows the partial fraction decomposition. Applying the substitution $\varepsilon = z + z^*$, binomial expansion and [42, eqs.(3.351.2) and (3.351.4)] into the following integral sequentially, we define

$$I_2(\varphi,z^*,\bar{\varphi},\mu) \triangleq \int_0^\infty \frac{z^\varphi}{(z+z^*)^{\bar{\varphi}}}\exp(-\mu z)dz$$
$$= \sum_{\varphi_3=0}^{\varphi}\binom{\varphi}{\varphi_3}(-z^*)^{\varphi-\varphi_3}\exp(\mu z^*)\int_{z^*}^\infty \varepsilon^{\varphi_3-\bar{\varphi}}\exp(-\mu\varepsilon)d\varepsilon$$
$$= \sum_{\varphi_3=0}^{\varphi}\binom{\varphi}{\varphi_3}(-z^*)^{\varphi-\varphi_3}\exp(\mu z^*)$$
$$\times \begin{cases} \exp(-\mu z^*)\sum_{\varphi_4=0}^{\varphi_3-\bar{\varphi}}\frac{(\varphi_3-\bar{\varphi})!(z^*)^{\varphi_4}}{\varphi_4!\mu^{\varphi_3-\bar{\varphi}-\varphi_4+1}}, & \varphi_3-\bar{\varphi}\geq 0, \\ \frac{-(-\mu)^{\bar{\varphi}-\varphi_3-1}\mathrm{Ei}(-\mu z^*)}{(\bar{\varphi}-\varphi_3-1)!} + \frac{\exp(-\mu z^*)}{(z^*)^{\bar{\varphi}-\varphi_3-1}} & \\ \times\sum_{\varphi_5=0}^{\bar{\varphi}-\varphi_3-2}\frac{(-\mu z^*)^{\varphi_5}(\bar{\varphi}-\varphi_3-\varphi_5-2)!}{(\bar{\varphi}-\varphi_3-1)!}, & \varphi_3-\bar{\varphi}<0, \end{cases} \quad (26)$$

where z^* is a constant. Thus, applying (26) and (23) into Θ_1 and Θ_2, respectively, we have $\Theta_1 = I_2(b,A,\bar{b},\frac{m_{s1}}{\alpha_1\rho_s\Omega_{s1}})$ and $\Theta_2 = I_1(b,\frac{m_{s1}}{\alpha_1\rho_s\Omega_{s1}},b_6)$. Substituting Θ_1 and Θ_2 into (25), we obtain C_{x_1}.

In the proposed scheme, U_1 must decode x_2 in t_1 to perform SIC, and the capacity of DF relaying is limited by the worst link [23]. Thus, the EC of x_2 can be expressed as $C_{x_2} = \frac{1}{4\ln 2}\int_0^\infty \frac{1-F_Q(q)}{1+q}dq$, where $Q = \min\{Q_1,Q_2,Q_3\}$ if SC is used, while $Q = \min\{Q_1,Q_2,Q_4\}$ when MRC is adopted. Based on this, the following theorem provides the closed-form expression of C_{x_2} for the proposed scheme.

Theorem 1: The closed-form expression of the ergodic capacity for x_2 can be given as

$$C_{x_2} = \begin{cases} C_{x_2}^{\mathrm{SC}}, & \text{for SC}, \\ C_{x_2}^{\mathrm{MRC}}, & \text{for MRC}, \end{cases} \quad (27)$$

where

$$C_{x_2}^{\mathrm{MRC}} \approx \frac{\alpha_2\pi}{8\alpha_1\ln 2}\sum_{n_1=1}^{N_1}\frac{\sqrt{1-\psi_{n_1}^2}}{N_1}$$
$$\times \frac{[1-\bar{F}_{Q_1}(q_{n_1})][1-\bar{F}_{Q_2}(q_{n_1})][1-F_{Q_4}(q_{n_1})]}{1+q_{n_1}}, \quad (28)$$

and $C_{x_2}^{\mathrm{SC}}$ can be given as (29), shown at the bottom of the next page. In (28) and (29), $\psi_{m_1} = \cos(\frac{2m_1-1}{2M_1}\pi)$, $q_{m_1} = \frac{\omega_4(1+\psi_{m_1})}{2\omega_3}$, $\psi_{m_2} = \cos(\frac{2m_2-1}{2M_2}\pi)$, $q_{m_2} = \frac{(1+\psi_{m_2})\alpha_2}{2\alpha_1} + \frac{(1-\psi_{m_2})\omega_4}{2\omega_3}$, $\psi_n = \cos(\frac{2n-1}{2N}\pi)$, $q_n = \frac{\alpha_2(1+\psi_n)}{2\alpha_1}$, $\psi_{n_1} = \cos(\frac{2n_1-1}{2N_1}\pi)$, $q_{n_1} = \frac{(1+\psi_{n_1})\alpha_2}{2\alpha_1}$, and M_1, M_2, N and N_1 represent complexity-accuracy tradeoff parameters. The functions $\bar{F}_{Q_1}(\cdot)$, $\bar{F}_{Q_2}(\cdot)$, $\bar{F}_{\bar{Q}_3}(\cdot)$, $\bar{F}_{\bar{Q}_4}(\cdot)$ and $F_{Q_4}(\cdot)$ are defined in Appendix A.

Proof: See Appendix A. ∎

Following the same steps in (24) and (25), we can use (18) to obtain the EC of x_3 as

$$C_{x_3} = \frac{\Delta_{i,i_1}}{4\ln 2}\Bigg\{\sum_{i_2=0}^{i_1+m_{r1}}-\left(\frac{1}{B-1}\right)^{i_2}I_2\left(i,B,\bar{i},\frac{m_{s1}}{\rho_s\Omega_{s1}}\right)$$
$$+\left(\frac{1}{B-1}\right)^{i_1+m_{r1}}I_1\left(i,\frac{m_{s1}}{\rho_s\Omega_{s1}},i_6\right)\Bigg\}, \quad (30)$$

where $\Delta_{i,i_1} = \frac{{m_{r1}}^{m_{r1}}}{\Omega_{r1}^{m_{r1}}\Gamma(m_{r1})}\sum_{i=0}^{m_{s1}-1}\sum_{i_1=0}^{i}\binom{i}{i_1}{\rho_s}^{i_1-i}\times\frac{(i_1+m_{r1}-1)!}{i!}(\frac{m_{s1}}{\Omega_{s1}})^{i-i_1-m_{r1}}{a_2}^{-m_{r1}}$, $\bar{i} = i_1 + m_{r1} - i_2 + 1$ and $B = \frac{m_{r1}\Omega_{s1}}{\Omega_{r1}a_2m_{s1}}$.

Similarly, we use (19) to calculate the EC of x_4 as

$$C_{x_4} = \frac{1}{4\ln 2}\sum_{w=0}^{m_{r2}-1}\left(\frac{m_{r2}}{a_2\rho_s\Omega_{r2}}\right)^w/w!$$
$$\times I_1\left(w,\frac{m_{r2}}{a_2\rho_s\Omega_{r2}},w_1\right). \quad (31)$$

B. Ergodic Capacities of Uplink Signals

Based on (10), (20) and (21), we obtain the EC of u_1 as

$$C_{u_1} = \frac{1}{4\ln 2}\sum_{j=0}^{m_{s1}-1}\left(\frac{m_{s1}}{\beta_1a_1\rho_s\Omega_{s1}}\right)^j/j!$$
$$\times I_1\left(j,\frac{m_{s1}}{\beta_1a_1\rho_s\Omega_{s1}},j_1\right). \quad (32)$$

Since the worse of h_{r2} and h_{sr} dominates the capacity of u_2, the EC of u_2 can be expressed as $C_{u_2} = \frac{1}{4\ln 2}\int_0^\infty \frac{1-F_{\bar{S}}(\bar{s})}{1+\bar{s}}d\bar{s}$, where $\bar{S}=\min\{S_1,S_2\}$.

When the BS performs perfect SIC (i.e., $\vartheta_2=0$) in t_3, the CDFs of S_1 and S_2 can be respectively written as

$$\begin{aligned}F_{S_1}(s_1) =& \int_0^\infty F_{\lambda_{r2}}\left(\frac{x\beta_1 s_1}{\beta_2}+\frac{s_1}{\beta_2 a_1\rho_s}\right)f_{\lambda_{r1}}(x)dx\\ =&1-\Delta_{k,k_1}{s_1}^{k}(s_1+D_1)^{-(k_1+m_{r1})}\\ &\times\exp\left(-\frac{m_{r2}s_1}{\beta_2 a_1\rho_s\Omega_{r2}}\right),\end{aligned} \tag{33}$$

$$\begin{aligned}F_{S_2}(s_2) =&1-\sum_{l=0}^{m_{sr}-1}\left(\frac{m_{sr}}{\omega_2 a_1\rho_s\Omega_{sr}}\right)^l\frac{{s_2}^l}{l!}\\ &\times\exp\left(-\frac{m_{sr}s_2}{\omega_2 a_1\rho_s\Omega_{sr}}\right),\end{aligned} \tag{34}$$

where $\Delta_{k,k_1}=\frac{{m_{r1}}^{m_{r1}}}{{\Omega_{r1}}^{m_{r1}}\Gamma(m_{r1})}\sum_{k=0}^{m_{r2}-1}\sum_{k_1=0}^{k}\binom{k}{k_1}(\frac{\beta_1}{\beta_2})^{-m_{r1}}\times\frac{(k_1+m_{r1}-1)!}{k!}(\beta_2 a_1\rho_s)^{k_1-k}(\frac{m_{r2}}{\Omega_{r2}})^{k-k_1-m_{r1}}$ and $D_1=\frac{m_{r1}\beta_2\Omega_{r2}}{m_{r2}\beta_1\Omega_{r1}}$. Using (33) and (34), we apply the order statistics to obtain the CDF of $\bar{S}$ as $F_{\bar{S}}(\bar{s})=1-(1-F_{S_1}(\bar{s}))(1-F_{S_2}(\bar{s}))$. With the aid of (22), we can calculate the EC of u_2 with perfect SIC as

$$\begin{aligned}C_{u_2}^{p} =& \frac{\Delta_{k,k_1}}{4\ln 2}\sum_{l=0}^{m_{sr}-1}\left(\frac{m_{sr}}{\omega_2 a_1\rho_s\Omega_{sr}}\right)^l/l!\\ \times&\underbrace{\int_0^\infty(\bar{s}+D_1)^{-(k_1+m_{r1})}(1+\bar{s})^{-1}\bar{s}^{k+l}\exp\left(-D_2\bar{s}\right)d\bar{s}}_{\Xi},\end{aligned} \tag{35}$$

where $D_2=\frac{m_{r2}}{\beta_2 a_1\rho_s\Omega_{r2}}+\frac{m_{sr}}{\omega_2 a_1\rho_s\Omega_{sr}}$. Following the same steps in (25), we have

$$\begin{aligned}\Xi =& \sum_{\delta_2=1}^{k_1+m_{r1}}-(D_1-1)^{-\delta_2}I_2(k+l,D_1,\bar{k},D_2)\\ &+(D_1-1)^{-(k_1+m_{r1})}I_1(k+l,D_2,\delta_3),\end{aligned} \tag{36}$$

where $\bar{k}=k_1+m_{r1}+1-\delta_2$. By plugging (36) into (35), we can obtain $C_{u_2}^{p}$.

Conversely, the following theorem gives the closed-form expression of C_{u_2} with imperfect SIC.

Theorem 2: When the BS performs imperfect SIC (i.e., $\vartheta_2\neq 0$) in t_3, the EC of u_2 can be written as (37), shown at the bottom of the page. In (37), $d_{\chi_1}^1=\frac{1}{(k_1+m_{r1}-\chi_1)!}\frac{\partial^{k_1+m_{r1}-\chi_1}}{\partial\bar{s}^{k_1+m_{r1}-\chi_1}}[\frac{1}{(\bar{s}+D_3)^{l_1+m_{s1}+1-\delta_1}}]|_{\bar{s}=-D_1}$, $\chi^*=l_1+m_{s1}+1-\delta_1$, $\delta^*=k_1+l_1+m_{r1}+m_{s1}$, $k^*=\delta^*+1-\delta_3$, $d_{\chi_2}^2=\frac{1}{(\chi^*-\chi_2)!}\frac{\partial^{\chi^*-\chi_2}}{\partial\bar{s}^{\chi^*-\chi_2}}[\frac{1}{(\bar{s}+D_1)^{k_1+m_{r1}}}]|_{\bar{s}=-D_3}$ and $D_3=\frac{\omega_2\Omega_{sr}m_{s1}}{m_{sr}\omega_3\vartheta_2\Omega_{s1}}$.

Proof: See Appendix B. ∎

Following the same steps in (24) and (25), we can use (14) to calculate the EC of u_3 as

$$\begin{aligned}C_{u_3} =&\frac{\Delta_{v,v_1}}{4\ln 2}\Big\{\sum_{v_2=0}^{v_1+m_{s1}}-\Big(\frac{1}{E-1}\Big)^{v_2}I_2\Big(v,E,\bar{v},\frac{m_{s1}}{\omega_3 a_1\rho_s\Omega_{s1}}\Big)\\ &+\Big(\frac{1}{E-1}\Big)^{v_1+m_{s1}}I_1\Big(v,\frac{m_{s1}}{\omega_3 a_1\rho_s\Omega_{s1}},v_3\Big)\Big\},\end{aligned} \tag{38}$$

where $\Delta_{v,v_1}=\frac{{m_{sr}}^{m_{sr}}}{{\Omega_{sr}}^{m_{sr}}\Gamma(m_{sr})}\sum_{v=0}^{m_{s1}-1}\sum_{v_1=0}^{v}\binom{v}{v_1}(\omega_2)^{-m_{sr}}\times\frac{(v_1+m_{sr}-1)!}{v!}(\frac{m_{s1}}{\omega_3\Omega_{s1}})^{v-v_1-m_{sr}}(a_1\rho_s)^{v_1-v}$, $\bar{v}=v_1+m_{s1}+1-v_2$ and $E=\frac{\omega_3 m_{sr}\Omega_{s1}}{\omega_2 m_{s1}\Omega_{sr}}$.

C. Average SE of the Proposed Scheme

The overall uplink and downlink ESCs are usually jointly evaluated to analyze the whole system performance in some specific scenarios such as two-way relay systems [43], CDRT [22] and full-duplex radios scenarios [44]. In this paper, we can directly calculate the average SE[3] using the overall ESC to characterize the SE gain achieved by the proposed scheme. Since the unit time and normalized bandwidth is adopted, we can use (21), (25), (27), (30), (31), (32), (35), (37) and (38) to obtain the average SE of the proposed scheme as

$$C_{\mathrm{SE}}^{\mathrm{Pro.}}=\begin{cases}\sum\limits_{\forall\theta\in\Psi}C_\theta+C_{x_1}^{p}+C_{u_2}^{p}, & \mathbf{\Pi 1},\\ \sum\limits_{\forall\theta\in\Psi}C_\theta+C_{x_1}+C_{u_2}, & \mathbf{\Pi 2},\end{cases} \tag{39}$$

[3]Note that the average SE of the proposed scheme can be maximized by the improved joint optimization scheme [45].

$$C_{x_2}^{\mathrm{SC}}\approx\begin{cases}\frac{\pi}{8\ln 2}\Big\{\frac{\omega_4}{\omega_3}\sum\limits_{m_1=1}^{M_1}\frac{\sqrt{1-\psi_{m_1}^2}}{M_1}\frac{[1-\bar{F}_{\bar{Q}_3}(q_{m_1})\bar{F}_{\bar{Q}_4}(q_{m_1})][1-\bar{F}_{Q_1}(q_{m_1})][1-\bar{F}_{Q_2}(q_{m_1})]}{1+q_{m_1}}\\ +\Big(\frac{\alpha_2}{\alpha_1}-\frac{\omega_4}{\omega_3}\Big)\sum\limits_{m_2=1}^{M_2}\frac{\sqrt{1-\psi_{m_2}^2}}{M_2}\frac{[1-\bar{F}_{\bar{Q}_4}(q_{m_2})][1-\bar{F}_{Q_1}(q_{m_2})][1-\bar{F}_{Q_2}(q_{m_2})]}{1+q_{m_2}}\Big\}, & \frac{\omega_4}{\omega_3}<\frac{\alpha_2}{\alpha_1},\\ \frac{\pi}{8\ln 2}\frac{\alpha_2}{\alpha_1}\sum\limits_{n=1}^{N}\frac{\sqrt{1-\psi_n^2}}{N}\frac{[1-\bar{F}_{\bar{Q}_3}(q_n)\bar{F}_{\bar{Q}_4}(q_n)][1-\bar{F}_{Q_1}(q_n)][1-\bar{F}_{Q_2}(q_n)]}{1+q_n}, & \frac{\omega_4}{\omega_3}\geq\frac{\alpha_2}{\alpha_1}.\end{cases} \tag{29}$$

$$C_{u_2}=\frac{\Delta_{k,k_1}\Delta_{l,l_1}}{4\ln 2}\times\begin{cases}\sum\limits_{\delta_1=1}^{l_1+m_{s1}}-(D_3-1)^{-\delta_1}\Big\{\sum\limits_{\chi_1=1}^{k_1+m_{r1}}d_{\chi_1}^1I_2(k+l,D_1,\chi_1,D_2)\\ +\sum\limits_{\chi_2=1}^{\chi^*}d_{\chi_2}^2I_2(k+l,D_3,\chi_2,D_2)\Big\}+(D_3-1)^{-(l_1+m_{s1})}\Xi, & D_1\neq D_3,\\ \sum\limits_{\delta_3=1}^{\delta^*}-(D_1-1)^{-\delta_3}I_2(k+l,D_1,k^*,D_2)+(D_1-1)^{-\delta^*}I_1(k+l,D_2,\delta_4), & D_1=D_3.\end{cases} \tag{37}$$

where $\Psi = \{x_2, x_3, x_4, u_1, u_3\}$, and $\mathbf{\Pi 1}$ and $\mathbf{\Pi 2}$ denote perfect SIC and imperfect SIC, respectively. Since the D2D message x_4 contributes to the overall system performance, C_{x_4} is also considered in (39) as in [30] and [31].

Next, we provide the asymptotic analysis for the average SE of the proposed scheme in the following theorem. We first define two functions as

$$I_3(\hat{\varphi},\hat{\mu},\hat{v}) \triangleq -\frac{1}{4\ln 2}\Big\{(1+\hat{\mu})(E^*+\ln(\hat{\mu})-\hat{\mu}) - \sum_{\hat{v}=1}^{\hat{\varphi}-1}(\hat{v}-1)!/\hat{v}!\Big\}, \tag{40a}$$

$$I_4(\hat{\varphi},\hat{\mu},\hat{v},\hat{z}_1^*,\hat{z}_2^*) \triangleq \frac{1}{4\ln 2}\hat{z}_1^{*-\hat{\mu}}\hat{z}_2^{*\hat{\varphi}+1-\hat{v}} \times \mathcal{B}(\hat{\varphi}+1,\hat{\mu}+\hat{v}-\hat{\varphi}-1) \times_2 \mathcal{F}_1(\hat{\mu},\hat{\varphi}+1;\hat{\mu}+\hat{v};1-\hat{z}_2^*/\hat{z}_1^*), \tag{40b}$$

where E^* is Euler constant, $\hat{z}_1^*$ and $\hat{z}_2^*$ are constants, and $\mathcal{B}(\cdot)$ and ${}_2\mathcal{F}_1(\cdot)$ denote Beta function and the generalized Hypergeometric function with order 2 and 1, respectively.

Theorem 3: When $\rho_s \to \infty$, an asymptotic expression for the average SE of the proposed scheme can be given as

$$\tilde{C}_{\mathrm{SE}}^{\mathrm{Pro.}} = \begin{cases} \sum\limits_{\forall\theta\in\Psi} \tilde{C}_\theta + \tilde{C}_{x_1}^p + \tilde{C}_{u_2}^p, & \mathbf{\Pi 1}, \\ \sum\limits_{\forall\theta\in\Psi} \tilde{C}_\theta + \tilde{C}_{x_1} + \tilde{C}_{u_2}, & \mathbf{\Pi 2}, \end{cases} \tag{41}$$

where $\tilde{C}_{x_1}^p = I_3(m_{s1}, \frac{m_{s1}}{\alpha_1\rho_s\Omega_{s1}}, \hat{b})$, $\tilde{C}_{x_1} = \hat{\Delta}_b I_4(b, b+m_{s1}, 1, A, 1)$, $\tilde{C}_{x_2} = \frac{1}{4\ln 2}\ln(\frac{\alpha_2}{\alpha_1})$, $\tilde{C}_{x_3} = \hat{\Delta}_i I_4(i, i+m_{r1}, 1, B, 1)$, $\tilde{C}_{x_4} = I_3(m_{r2}, \frac{m_{r2}}{a_2\rho_s\Omega_{r2}}, \hat{w})$, $\tilde{C}_{u_1} = I_3(m_{s1}, \frac{m_{s1}}{\beta_1 a_1\rho_s\Omega_{s1}}, \hat{j})$, $\tilde{C}_{u_2}^p = \hat{\Delta}_k I_4(k, k+m_{r1}, 1, D_1, 1)$ and $\tilde{C}_{u_3} = \hat{\Delta}_v I_4(v, v+m_{sr}, 1, E, 1)$. $\tilde{C}_{u_2}$ is shown in (42) at the bottom of the page, where

$$\hat{k} = k + m_{r1} + 1 - \delta_2, \tag{43a}$$

$$\hat{\Delta}_b = \Big(\frac{\alpha_1}{\alpha_2\vartheta_1}\Big)^{m_{s1}} \sum_{b=0}^{m_{s1}-1} \frac{(b+m_{s1}-1)!}{b!\Gamma(m_{s1})}, \tag{43b}$$

$$\hat{\Delta}_i = \Big(\frac{m_{r1}\Omega_{s1}}{a_2 m_{s1}\Omega_{r1}}\Big)^{m_{r1}} \sum_{i=0}^{m_{s1}-1} \frac{(i+m_{r1}-1)!}{i!\Gamma(m_{r1})}, \tag{43c}$$

$$\hat{\Delta}_v = \Big(\frac{\omega_3 m_{sr}\Omega_{s1}}{\omega_2 m_{s1}\Omega_{sr}}\Big)^{m_{sr}} \sum_{v=0}^{m_{s1}-1} \frac{(v+m_{sr}-1)!}{v!\Gamma(m_{sr})}, \tag{43d}$$

$$\hat{\Delta}_k = \Big(\frac{\beta_2 m_{r1}\Omega_{r2}}{\beta_1 m_{r2}\Omega_{r1}}\Big)^{m_{r1}} \sum_{k=0}^{m_{r2}-1} \frac{(k+m_{r1}-1)!}{k!\Gamma(m_{r1})}, \tag{43e}$$

$$\hat{\Delta}_l = \Big(\frac{\omega_2 m_{s1}\Omega_{sr}}{\omega_3\vartheta_2 m_{sr}\Omega_{s1}}\Big)^{m_{s1}} \sum_{l=0}^{m_{sr}-1} \frac{(l+m_{s1}-1)!}{l!\Gamma(m_{s1})}. \tag{43f}$$

Proof: See Appendix C. ∎

D. Benchmark Schemes

Three schemes, including a conventional NCDRT (C-NCDRT) scheme and two OMA schemes, are studied as benchmarks under same parameters for fair comparison.

1) C-NCDRT Scheme: Using downlink NCDRT in [23] and uplink NCDRT in [27], the closed-form expression of the average SE for C-NCDRT is given by

$$C_{\mathrm{SE}}^{\mathrm{Con.}} = \begin{cases} \sum\limits_{\forall\theta_1\in\Psi_1} C_{\theta_1}^{\mathrm{Con.}} + C_{x_1}^{\mathrm{Con.},p} + C_{u_2}^{\mathrm{Con.},p}, & \mathbf{\Pi 1}, \\ \sum\limits_{\forall\theta_1\in\Psi_1} C_{\theta_1}^{\mathrm{Con.}} + C_{x_1}^{\mathrm{Con.}} + C_{u_2}^{\mathrm{Con.}}, & \mathbf{\Pi 2}, \end{cases} \tag{44}$$

where $\Psi_1 = \{x_2, x_3, u_1, u_3\}$, $C_{x_1}^{\mathrm{Con.},p} = C_{x_1}^p$, $C_{u_1}^{\mathrm{Con.}} = C_{u_1}$, $C_{x_1}^{\mathrm{Con.}} = C_{x_1}$, $C_{u_3}^{\mathrm{Con.}} = C_{u_3}(\omega_3 \Rightarrow \omega_3+\omega_4, \omega_2 \Rightarrow \omega_1+\omega_2)$, $C_{x_3}^{\mathrm{Con.}} = C_{x_1}^p(\alpha_1 \Rightarrow 1)$, $C_{u_2}^{\mathrm{Con.},p} = C_{u_2}^p(\omega_2 \Rightarrow \omega_1+\omega_2, \omega_3 \Rightarrow \omega_3+\omega_4)$, $C_{u_2}^{\mathrm{Con.}} = C_{u_2}(\omega_3 \Rightarrow \omega_3+\omega_4)$, $C_{x_2}^{\mathrm{Con.}} = \sum_{m=1}^{M}\sqrt{1-\psi_m^2}\frac{\tau\alpha_2\pi}{2M}\frac{(\alpha_2-q_m)^{g_3}}{1-q_m}(\frac{\alpha_2}{q_m}-1)^{g_1+g_2} \times \exp(-(\frac{m_{s1}}{\rho_s\Omega_{s1}}+\frac{m_{sr}}{\rho_s\Omega_{sr}})\frac{\alpha_2}{\alpha_1 q_m}+\frac{m_{r2}q_m}{a_2\rho_s\Omega_{r2}\alpha_1})$, $\tau = \frac{1}{4\ln 2} \times \sum_{g_1=0}^{m_{s1}-1}\sum_{g_2=0}^{m_{sr}-1}\sum_{g_3=0}^{m_{r2}-1}(\frac{m_{sr}}{\Omega_{sr}})^{g_2}(\frac{m_{r2}}{a_2\Omega_{r2}})^{g_3}(\frac{1}{\alpha_1\rho_s})^{g_1+g_2+g_3} \times (\frac{m_{s1}}{\Omega_{s1}})^{g_1}/(g_1!g_2!g_3!)\exp((\frac{m_{s1}}{\rho_s\Omega_{s1}}+\frac{m_{sr}}{\rho_s\Omega_{sr}})\frac{1}{\alpha_1}-\frac{m_{r2}}{a_2\rho_s\Omega_{r2}}\frac{\alpha_2}{\alpha_1})$ and $C_A = C_B(a \Rightarrow b)$ denotes the operation to obtain C_A after replacing all a in C_B with b.

2) OMA-I: This scheme uses eight phases in TDMA to complete the transmission of six signals in C-NCDRT. Based on (21), (23) and (32), we derive the average SE of OMA-I as

$$\begin{aligned} C_{\mathrm{SE}}^{\mathrm{OMA-I}} &= C_{x_1}^p(\alpha_1 \Rightarrow 1) + C_{u_1}(\beta_1 \Rightarrow 1) \\ &+ \frac{1}{8\ln 2}\sum_{b=0}^{m_{r2}-1}\sum_{b_1=0}^{m_{sr}-1}\Big(\frac{m_{r2}}{\rho_s\Omega_{r2}}\Big)^b\Big(\frac{m_{sr}}{\rho_s\Omega_{sr}}\Big)^{b_1}\frac{1}{b!b_1!} \\ &\times\Big\{\Big(\frac{1}{a_2}\Big)^b I_1\Big(b+b_1, \frac{m_{r2}}{a_2\rho_s\Omega_{r2}}+\frac{m_{sr}}{\rho_s\Omega_{sr}}, b_3\Big) \\ &+\Big(\frac{1}{a_1}\Big)^{b+b_1} I_1\Big(b+b_1, \frac{m_{r2}}{a_1\rho_s\Omega_{r2}}+\frac{m_{sr}}{a_1\rho_s\Omega_{sr}}, b_3\Big)\Big\}. \end{aligned} \tag{45}$$

3) OMA-II: Unlike OMA-I, OMA-II aims to transmit seven signals sent in the proposed scheme with nine phases. Based on (31) and (45), the average SE of OMA-II can be written as $C_{\mathrm{SE}}^{\mathrm{OMA-II}} = \frac{8}{9}C_{\mathrm{SE}}^{\mathrm{OMA-I}} + \frac{4}{9}C_{x_4}$.

E. User Fairness

In NOMA systems, performing SIC causes different users to achieve unequal rates. Thus, user fairness is a crucial measure to evaluate system performance. In this paper, the fairness of the proposed scheme can be analyzed via the commonly used Jain's fairness index [46]. Specifically, the Jain's fairness index for the uplink and downlink transmissions of the proposed scheme can be written as

$$\tilde{C}_{u_2} = \hat{\Delta}_k\hat{\Delta}_l \times \begin{cases} \sum\limits_{\delta_2=1}^{k+m_{r1}} -(D_1-1)^{-\delta_2} I_4(k+l, l+m_{s1}, \hat{k}, D_3, D_1) \\ +(D_1-1)^{-(k+m_{r1})} I_4(k+l, l+m_{s1}, 1, D_3, 1), & D_1 \neq D_3, \\ I_4(k+l, k+l+m_{r1}+m_{s1}, 1, D_1, 1), & D_1 = D_3. \end{cases} \tag{42}$$

$$\mathcal{J}_{\mathrm{D}}^{\mathrm{Pro.}} = \begin{cases} \frac{(C_{x_1}^p + C_{x_2} + C_{x_3} + C_{x_4})^2}{2((C_{x_1}^p + C_{x_3})^2 + (C_{x_2} + C_{x_4})^2)}, & \mathbf{\Pi_1}, \\ \frac{(C_{x_1} + C_{x_2} + C_{x_3} + C_{x_4})^2}{2((C_{x_1} + C_{x_3})^2 + (C_{x_2} + C_{x_4})^2)}, & \mathbf{\Pi_2}, \end{cases} \tag{46}$$

$$\mathcal{J}_{\mathrm{U}}^{\mathrm{Pro.}} = \begin{cases} \frac{(C_{u_1} + C_{u_2}^p + C_{u_3})^2}{2((C_{u_1} + C_{u_3})^2 + (C_{u_2}^p)^2)}, & \mathbf{\Pi_1}, \\ \frac{(C_{u_1} + C_{u_2} + C_{u_3})^2}{2((C_{u_1} + C_{u_3})^2 + (C_{u_2})^2)}, & \mathbf{\Pi_2}. \end{cases} \tag{47}$$

Note that the index range is 0 to 1, and a fairer system has a larger index. Similarly, the Jain's fairness index for other three benchmarks can be obtained by using the above SE analysis.

F. Energy Efficiency Gain

To investigate the EE of the proposed scheme (Pro.), we define the EE gain of the proposed scheme over the benchmarks (Ben.) as

$$\eta_{\mathrm{Ben.}}^{\mathrm{Pro.}} = \left(\frac{C_{\mathrm{SE}}^{\mathrm{Pro.}}}{P_{\mathrm{total}}^{\mathrm{Pro.}}} - \frac{C_{\mathrm{SE}}^{\mathrm{Ben.}}}{P_{\mathrm{total}}^{\mathrm{Ben.}}} \right) / \frac{C_{\mathrm{SE}}^{\mathrm{Ben.}}}{P_{\mathrm{total}}^{\mathrm{Ben.}}}, \tag{48}$$

where Ben. denotes the benchmarks (i.e., C-NCDRT, OMA-I and OMA-II), $P_{\mathrm{total}}^{\mathrm{Pro.}}$ and $P_{\mathrm{total}}^{\mathrm{Ben.}}$ represent the total energy consumption for the proposed scheme and the benchmarks, respectively. Specifically, we have $P_{\mathrm{total}}^{\mathrm{Pro.}} = P_{\mathrm{total}}^{\mathrm{Con.}} = (2P_s + P_r + 2P_u)/4 + P_c$, $P_{\mathrm{total}}^{\mathrm{OMA-I}} = (3P_s + P_r + 4P_u)/8 + P_c$ and $P_{\mathrm{total}}^{\mathrm{OMA-II}} = (3P_s + 2P_r + 4P_u)/9 + P_c$, where P_c is the circuit power consumption.

V. Numerical Results And Discussion

In this section, the performances of the proposed scheme (Pro.), the conventional scheme (Con.), OMA-I and OMA-II, in terms of ESC, average SE, user fairness and EE gain are compared. In the comparison, we consider a BS directly transmits information to a cell-center user, and it communicates with a cell-edge user via a DF relaying user. Specifically, we set $d_{sr} = d_{r1} = d_{12} = 50$ m, $d_{s1} = 10$ m and $d_{r2} = 5$ m, which follows the construction regulations of the triangle. Without loss of generality, we assume that the PA coefficients are $\alpha_1 = 0.05$, $\alpha_2 = 0.95$, $\beta_1 = 0.4$, $\beta_2 = 0.6$, $\omega_1 = 0.35$, $\omega_2 = 0.05$, $\omega_3 = 0.25$, $\omega_4 = 0.35$ and the scale factors are $a_1 = a_2 = 0.1$. Then, we assume $\Omega_{\tilde{x}\tilde{y}} = \tilde{h}_0 d_{\tilde{x}\tilde{y}}^{-\zeta}$, where $\tilde{h}_0$ denotes the channel gain for reference distance $d = 1$ m and ζ is the path-loss exponent. In addition, we set $\zeta = 3$, $\tilde{h}_0 = -30$ dB and $N_0 = -110$ dBm. The circuit power consumption P_c is assumed to be 1 W for illustration purpose [47].

A. ESC for Downlink Signals

Fig. 3 depicts the ESC of downlink signals versus the transmit power of BS with perfect SIC for different channel fading parameter settings (i.e., $m_{\tilde{x}\tilde{y}} = 1$ and $m_{\tilde{x}\tilde{y}} = 2$). The figure verifies that the simulation curves agree with the corresponding analytical ones perfectly. It is shown that the proposed scheme can achieve the highest ESC for downlink transmission among the four schemes. This is because the proposed scheme can transmit more downlink signals using the same time resource. Since C_{x_2} is determined by the minimum of Q_1, Q_2 and Q_3 (or Q_4), the proposed scheme using SC (Pro-SC.) can achieve the same ESC for downlink signals compared with using MRC (Pro-MRC.). Moreover, NOMA-based schemes (i.e., the proposed scheme and the conventional one) adopting perfect SIC can obtain better ESC performance than OMA schemes, which proves the higher SE potential of NOMA. Meanwhile, the ESC of downlink transmission for OMA-II is better than that for OMA-I. The reason is that OMA-II can transmit one more downlink signal (i.e., x_4) using the same time resource. Besides, the slight lower ESC is obtained when $m_{\tilde{x}\tilde{y}} = 1$, as expected, as the Rayleigh fading channel is worse than other conditions (i.e., $m_{\tilde{x}\tilde{y}} \neq 1$).

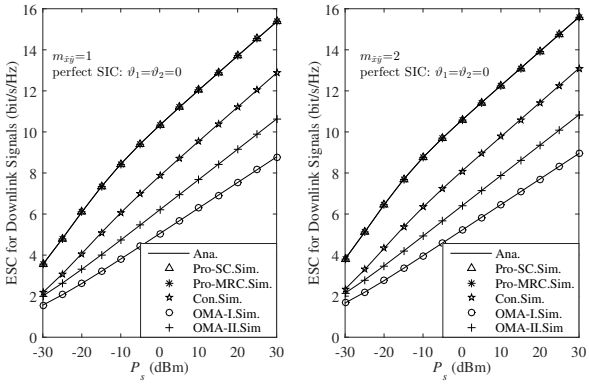

Fig. 3. ESC for downlink signals versus P_s under perfect SIC, with two cases of $m_{\tilde{x}\tilde{y}} = 1$ and $m_{\tilde{x}\tilde{y}} = 2$ considered.

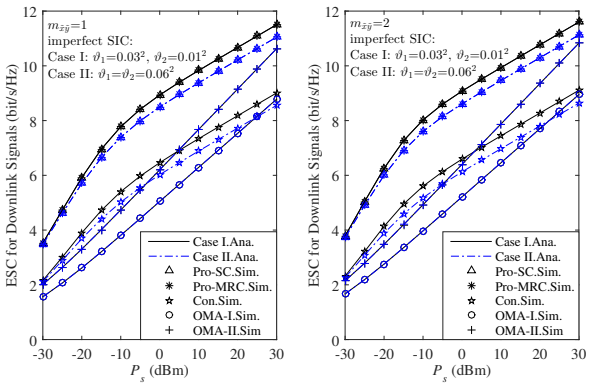

Fig. 4. ESC for downlink signals versus P_s under imperfect SIC, with different ϑ_1, ϑ_2 and $m_{\tilde{x}\tilde{y}}$ considered.

Fig.4 plots the relationship between the ESC for downlink signals and the transmit power of BS with imperfect SIC. The analytical results are verified by the simulation ones. The figure demonstrates that the ESC for downlink signals attained by the NOMA-based schemes decreases with an increase in the interference level of imperfect SIC. Also, OMA schemes are not affected by imperfect SIC, since no SIC is required in OMA schemes. Even with the imperfect SIC, the proposed scheme can still provide the best ESC performance with acceptable imperfect SIC level (i.e., $\vartheta_1 = 0.03^2, \vartheta_2 = 0.01^2$ and $\vartheta_1 = \vartheta_2 = 0.06^2$). However, in the high P_s regime, the ESC of the downlink signals for the conventional scheme becomes worse than OMA schemes due to imperfect SIC.

B. ESC for Uplink Signals

Fig. 5 illustrates the ESC for uplink signals versus the transmit power of BS with perfect SIC. It is observed that the analytical results match the corresponding simulations

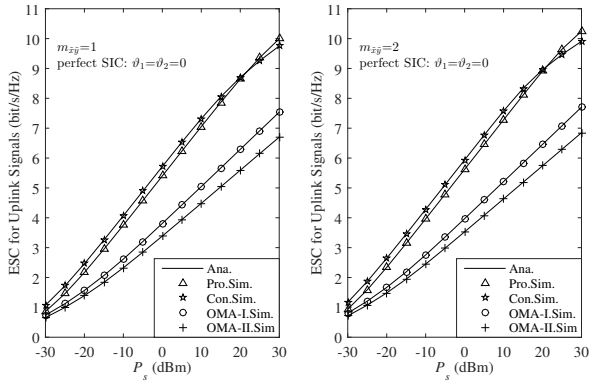

Fig. 5. ESC for uplink signals versus P_s under perfect SIC, with two cases of $m_{\tilde{x}\tilde{y}} = 1$ and $m_{\tilde{x}\tilde{y}} = 2$ considered.

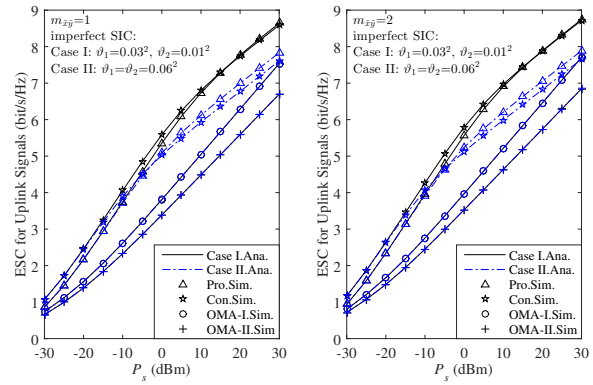

Fig. 6. ESC for uplink signals versus P_s under imperfect SIC, with different ϑ_1, ϑ_2 and $m_{\tilde{x}\tilde{y}}$ considered.

perfectly. Moreover, it is interesting to find that the ESC of uplink transmission for the proposed scheme is slightly worse than that for the conventional one in the low-medium P_s, and it becomes slightly better than the conventional scheme for high P_s. This is because in the third phase, the proposed scheme allocates a part of uplink transmit power to transmit x_2, leading to slight performance loss for low-medium P_s. However, as the transmit power of BS increases, the performance gap between the proposed scheme and the conventional one becomes smaller due to the inherent characteristic of the interference-limit system and PA settings. Compared with OMA schemes, the proposed scheme achieves better performance with perfect SIC. Moreover, the ESC of uplink transmission for OMA-I is higher than that for OMA-II, for that in the uplink transmission, OMA-II consumes less time than OMA-I to transmit the same signals.

Fig. 6 shows the relationship between the ESC achieved in uplink transmission and the transmit power of BS under imperfect SIC. As expected, the interference level of imperfect SIC affects the performance of NOMA-based schemes significantly. For example, the ESC corresponding to $\vartheta_2 = 0.01^2$ is better than that with $\vartheta_2 = 0.06^2$. In Fig. 6, the phenomenon between the proposed scheme and the conventional one can be explained as the same reasons provided in Fig. 5. Although NOMA-based schemes outperform than OMA schemes in terms of the ESC for uplink transmission in this figure, it

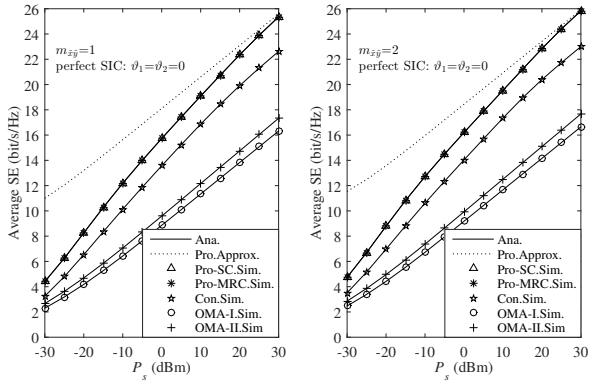

Fig. 7. Comparison of average SE for the proposed scheme and three benchmarks versus P_s under perfect SIC, with two cases of $m_{\tilde{x}\tilde{y}} = 1$ and $m_{\tilde{x}\tilde{y}} = 2$ considered.

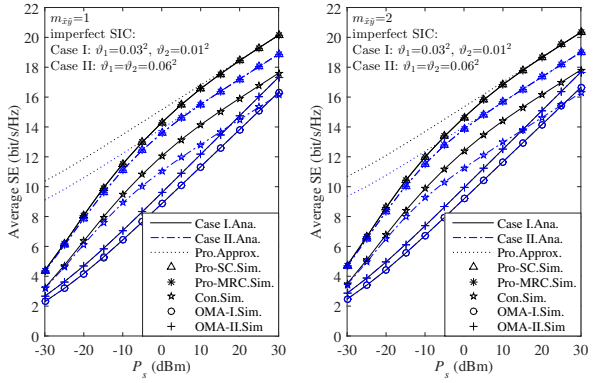

Fig. 8. Comparison of average SE for the proposed scheme and three benchmarks versus P_s under imperfect SIC, with different ϑ_1, ϑ_2 and $m_{\tilde{x}\tilde{y}}$ considered.

can be predicted that the increase of interference caused by imperfect SIC will make the performance of NOMA-based schemes worse than that of OMA schemes. Thus, a well-designed SIC receiver is crucial for NOMA to improve the SE.

C. Average SE for the Proposed Scheme

Fig. 7 demonstrates the average SE of the proposed scheme versus the transmit power of BS for different fading parameters with perfect SIC. In this figure, the derived results in (39), (44) and (45) match well with the corresponding simulations. Besides, the asymptotic analysis for the average SE of the proposed scheme agrees well with the exact one for high P_s, and becomes tight as P_s increases, which is consistent with *Theorem 3*. It can be seen that the proposed scheme can achieve better ESC than the conventional benchmark with perfect SIC. This is because the proposed scheme can transmit more information using the same time resource, which can effectively enhance the SE. Because Pro-SC. can achieve the same EC of x_2 with Pro-MRC., the average SE of Pro-SC. equals that of Pro-MRC.. Compared with OMA schemes, adopting NOMA with perfect SIC can effectively improve the SE.

Fig. 8 provides the average SE according to the transmit power of BS with imperfect SIC. Similarly, performing im-

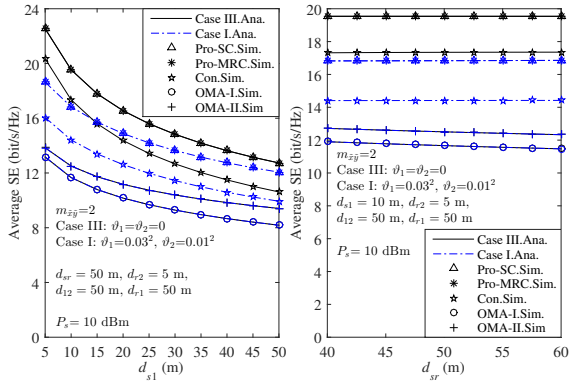

(a) (b)

Fig. 9. (a) Average SE according to the distance d_{s1}. (b) Average SE according to the distance d_{sr}.

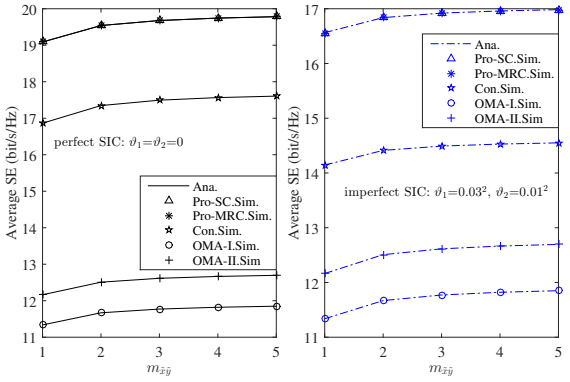

(a) (b)

Fig. 10. (a) Average SE according to $m_{\tilde{x}\tilde{y}}$, with $\vartheta_1 = \vartheta_2 = 0$ considered. (b) Average SE according to $m_{\tilde{x}\tilde{y}}$, with $\vartheta_1 = 0.03^2$ and $\vartheta_2 = 0.01^2$ considered.

perfect SIC may decrease the average SE of both proposed and conventional schemes. But even so, the superiority of the proposed scheme over the other three benchmarks can still be maintained with an acceptable degree of imperfect SIC. For example, when $\vartheta_1 = \vartheta_2 = 0.06^2$, the average SE of the proposed scheme is the best among all schemes, while the average SE of the conventional scheme becomes lower than OMA-II as P_s increases due to the imperfect SIC. This means that the proposed scheme is more robust to imperfect SIC than the conventional one. Meanwhile, this figure verifies the effectiveness of the proposed scheme with imperfect SIC as well as the correctness of the exact analysis and asymptotic one.

Fig. 9 illustrates that the proposed scheme can achieve the best average SE among all schemes for different d_{sr} and d_{s1}. Fig. 9(a) shows that the average SE for all comparisons decreases as d_{s1} increases, due to the fact that the worse h_{s1} can decrease the achievable capacities of x_1, x_3, u_1 and u_3 for all schemes. Besides, the increase of d_{s1} makes the channel difference between h_{s1} and h_{sr} become smaller, which also decreases the average SE of the proposed scheme and the conventional one. In Fig. 9(b), as d_{sr} increases, the average SE for both the proposed scheme and the conventional one remains stable while the average SE of OMA-I and OMA-II becomes worse. This is because the increase of d_{sr} decreases the EC of x_2 and u_2, as well as increasing the EC of u_1 due to the decrease of the interference from R. However, the same benefit of decreasing interference does not exist in OMA-I and OMA-II, which decreases the average SE of these two schemes.

Fig. 10 shows the impact of the fading parameter m on the average SE. In Fig. 10, the proposed scheme can achieve the best average SE among all comparisons. Moreover, the increase of m can improve the average SE for all schemes. This is because the channel condition becomes better when m is larger. Interestingly, the impact of m on the average SE becomes smaller when m increases. There are two reasons accountable for this phenomenon. 1) Based on the above theoretical analysis, the average SE is determined by the fading parameter m, the pathloss (i.e., $\Omega_{\tilde{x}\tilde{y}}$) and the PA. Although the average SE can be marginally affected by the fading parameter m, it is mainly dominated by the pathloss and the PA. 2) When $\Omega_{\tilde{x}\tilde{y}}$ and PA are fixed, the difference of the average SE with different m is insignificant, which is consistent with the results in [48] and [49].

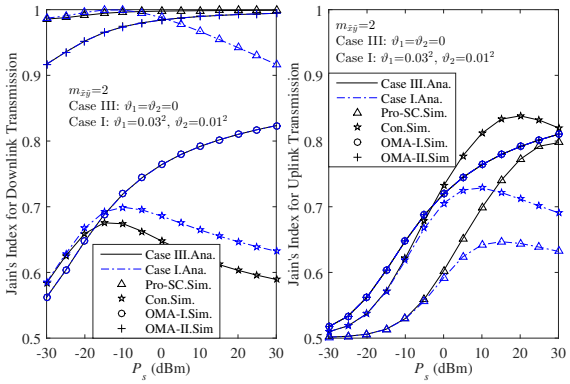

(a) (b)

Fig. 11. (a) Fairness comparison for downlink transmission. (b) Fairness comparison for uplink transmission.

D. User Fairness

Fig. 11 provides the Jain's fairness index for downlink and uplink transmissions versus the transmit power of BS. In Fig. 11(a), the proposed scheme with perfect SIC can achieve the best fairness for downlink transmission, because it can improve the achievable capacity of U_2 by transmitting x_4. However, as P_s increases, the fairness of the proposed scheme with imperfect SIC rises first and then decreases. The fairness curves of the conventional scheme with both perfect and imperfect SIC have similar trends. This is because imperfect SIC affects the EC of x_1, and the increase of P_s decreases the EC gap between U_1 and U_2 when P_s is small. For larger P_s, the EC of downlink transmission for both U_1 and U_2 are limited by the PAs, increasing the EC gap. Since OMA schemes are interference-free systems, their fairness increases as P_s increases. Fig. 11(b) shows that the fairness for uplink transmission of the proposed scheme is worse than that of the conventional scheme. This is because the proposed scheme uses a portion of uplink transmit power to send x_2 in the third

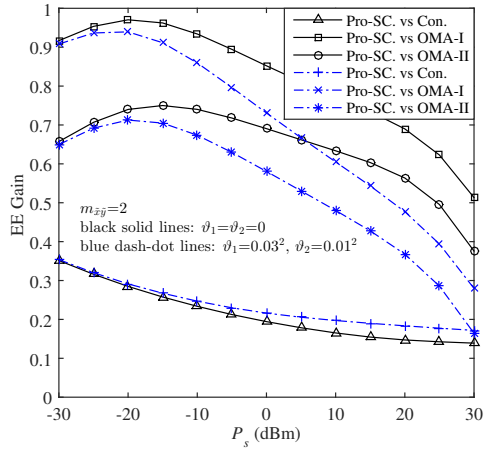

Fig. 12. EE gain versus P_s, with two cases of $\vartheta_1 = \vartheta_2 = 0$ and $\vartheta_1 = 0.03^2, \vartheta_2 = 0.01^2$ considered. $m_{\tilde{x}\tilde{y}}$=2.

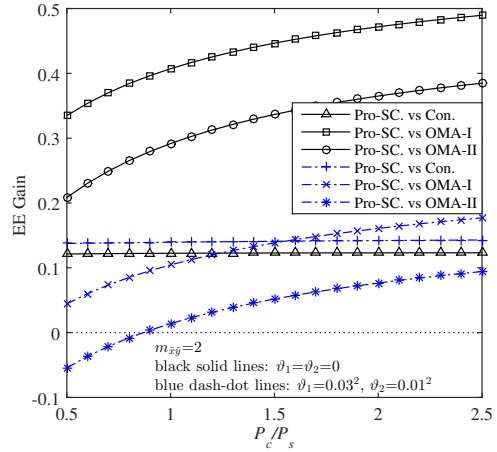

Fig. 13. EE gain versus P_c/P_s, with two cases of $\vartheta_1 = \vartheta_2 = 0$ and $\vartheta_1 = 0.03^2, \vartheta_2 = 0.01^2$ considered. $m_{\tilde{x}\tilde{y}}$=2.

phase, increasing the EC gap between U_1 and U_2. Since the uplink EC of OMA-I is linearly proportional to that of OMA-II, OMA-I has the same uplink fairness with OMA-II.

E. EE Gain

In Fig. 12, we provide the EE gain of the proposed scheme over other benchmarks versus the transmit power of BS. It shows that the proposed scheme can achieve better EE over the other existing schemes with perfect SIC. However, the EE gain of the proposed scheme over the conventional one approaches a lower limit as P_s increases. This is because there is a constant scaling relationship between the average SE and P_s for both the proposed and conventional schemes in the high P_s regime. Compared with OMA schemes, NOMA is an interference-limited system. Thus, the EE gains of the proposed scheme over OMA schemes decrease for high P_s. Besides, in the high P_s regime, the EE gains achieved by the proposed scheme over OMA schemes decrease when the interference caused by imperfect SIC increases, which is consistent with the discussion in Fig. 8.

In Fig. 13, we provide the EE gain versus P_c/P_s, where the circuit power consumption is 1 W. It is demonstrated that the EE gains obtained by the proposed scheme over OMA schemes increase as P_c/P_s increases. The reason is that when P_s decreases, $P_{\text{total}}^{\text{OMAs}}/P_{\text{total}}^{\text{Pro.}}$ becomes lager but $C_{\text{SE}}^{\text{Pro.}}/C_{\text{SE}}^{\text{OMAs}}$ keeps constant, which is consistent with (48). It is interesting to find that the EE of OMA-II is better than the proposed scheme when $\vartheta_1 = 0.03^2, \vartheta_2 = 0.01^2$ and $P_c/P_s \leq 0.8$. An intuitive explanation is that the effect of imperfect SIC decreases the system SE of the proposed scheme. Besides, the EE gain of the proposed scheme over the conventional one is only determined by $C_{\text{SE}}^{\text{Pro.}}/C_{\text{SE}}^{\text{Con.}}$ due to $P_{\text{total}}^{\text{Pro.}}$=$P_{\text{total}}^{\text{Con.}}$, which keeps the corresponding curves stable as P_c/P_s increases.

VI. Conclusion

In this paper, we have investigated a CDRT system over Nakagami-m fading channels, where the BS can directly communicate with the CCU, while it needs the help of the relay and the CCU to communicate with the CEU. To further improve the SE, we proposed a spectrum-efficient scheme, in which the uplink and downlink transmissions are designed jointly via network coding. To characterize the system performance, we first derived the closed-form expressions of the average SE, the user fairness index and the EE for the proposed and other three comparison schemes with both perfect and imperfect SIC. Then, the asymptotic analysis of the average SE for the proposed scheme was also attained. Simulations were provided to verify the correctness of the analytical results and demonstrate the advantage of the proposed scheme in both SE and EE. In future work, we will focus on the PA optimization for maximizing the average SE of the proposed scheme.

VII. Acknowledgment

The authors sincerely thank the editor and anonymous reviewers for their detailed reviews and valuable comments, which have significantly improve the quality of the paper.

Appendix A
Proof of Theorem 1

Similar to (24), the CDFs of $Q_d, d \in \{1, 2\}$, are written as

$$F_{Q_d}(q_d) = \begin{cases} \bar{F}_{Q_d}(q_d) \triangleq 1 - \sum\limits_{g_d=0}^{m_d-1} \left(\frac{m_d}{\Omega_d}\right)^{g_d} \\ \times 1/g_d! \left(\frac{q_d}{(\alpha_2 - \alpha_1 q_d)\rho_s}\right)^{g_d} \\ \times \exp\left(-\frac{m_d q_d}{(\alpha_2 - \alpha_1 q_d)\rho_s \Omega_d}\right), & \frac{\alpha_2}{\alpha_1} > q_d, \\ 1, & \frac{\alpha_2}{\alpha_1} \leq q_d, \end{cases} \tag{49}$$

where $m_1 = m_{s1}$, $m_2 = m_{sr}$, $\Omega_1 = \Omega_{s1}$ and $\Omega_2 = \Omega_{sr}$. Let $Q_3 = \max\{\bar{Q}_3, \bar{Q}_4\}$, where $\bar{Q}_3 = \frac{\lambda_{12}\omega_4 a_1 \rho_s}{\lambda_{12}\omega_3 a_1 \rho_s + 1}$ and $\bar{Q}_4 = \lambda_{r2}\omega_1 a_1 \rho_s$. Thus, the CDF of Q_3 can be obtained by implementing the order statistics as

$$F_{Q_3}(q_3) = \begin{cases} \bar{F}_{\bar{Q}_3}(q_3)\bar{F}_{\bar{Q}_4}(q_3), & \frac{\omega_4}{\omega_3} > q_3, \\ \bar{F}_{\bar{Q}_4}(q_3), & \frac{\omega_4}{\omega_3} \leq q_3, \end{cases} \tag{50}$$

where $\bar{F}_{\bar{Q}_3}(q_3) \triangleq 1 - \sum_{g_3=0}^{m_{12}-1} (\frac{m_{12}}{\Omega_{12}})^{g_3}/g_3! (\frac{q_3}{a_1\rho_s(\omega_4 - \omega_3 q_3)})^{g_3} e^{-\frac{m_{12}}{\Omega_{12}} \frac{q_3}{a_1\rho_s(\omega_4 - \omega_3 q_3)}}$ and $\bar{F}_{\bar{Q}_4}(q_3) \triangleq 1 - \sum_{g_4=0}^{m_{r2}-1} (\frac{m_{r2}}{\Omega_{r2}})^{g_4}/g_4! (\frac{q_3}{\omega_1 a_1 \rho_s})^{g_4} e^{-\frac{m_{r2} q_3}{\omega_1 a_1 \rho_s \Omega_{r2}}}$. Applying (49) and (50) to the order

statistics of $F_Q(q) = 1-(1-F_{Q_1}(q))(1-F_{Q_2}(q))(1-F_{Q_3}(q))$, we can easily obtain the CDF of Q. Thus, when the proposed scheme uses SC at U_2, the EC of x_2 can be expressed as $C_{x_2}^{\mathrm{SC}} = \frac{1}{4\ln 2}\int_0^{\infty}\frac{1-F_Q(q)}{1+q}dq$. When $\frac{\omega_4}{\omega_3} < \frac{\alpha_2}{\alpha_1}$, we rewrite $C_{x_2}^{\mathrm{SC}}$ as

$$\begin{aligned}
&C_{x_2}^{\mathrm{SC}}\\
&= \frac{1}{4\ln 2}\Bigg\{\int_{\frac{\omega_4}{\omega_3}}^{\frac{\alpha_2}{\alpha_1}}\frac{[1-\bar{F}_{\bar{Q}_4}(q)][1-\bar{F}_{Q_1}(q)][1-\bar{F}_{Q_2}(q)]}{1+q}dq\\
&+\int_0^{\frac{\omega_4}{\omega_3}}\frac{[1-\bar{F}_{\bar{Q}_3}(q)\bar{F}_{\bar{Q}_4}(q)][1-\bar{F}_{Q_1}(q)][1-\bar{F}_{Q_2}(q)]}{1+q}dq\Bigg\}. \quad (51)
\end{aligned}$$

Since the integrations in (51) are mathematically intractable, we use Gaussian-Chebyshev quadrature to obtain an approximation as

$$\begin{aligned}
&C_{x_2}^{\mathrm{SC}}\\
&\approx \frac{\pi}{8\ln 2}\Bigg\{\frac{\omega_4}{\omega_3}\sum_{m_1=1}^{M_1}\frac{\sqrt{1-\psi_{m_1}^2}}{M_1}\\
&\times\frac{[1-\bar{F}_{\bar{Q}_3}(q_{m_1})\bar{F}_{\bar{Q}_4}(q_{m_1})][1-\bar{F}_{Q_1}(q_{m_1})][1-\bar{F}_{Q_2}(q_{m_1})]}{1+q_{m_1}}\\
&+\left(\frac{\alpha_2}{\alpha_1}-\frac{\omega_4}{\omega_3}\right)\sum_{m_2=1}^{M_2}\frac{\sqrt{1-\psi_{m_2}^2}}{M_2}\\
&\times\frac{[1-\bar{F}_{\bar{Q}_4}(q_{m_2})][1-\bar{F}_{Q_1}(q_{m_2})][1-\bar{F}_{Q_2}(q_{m_2})]}{1+q_{m_2}}\Bigg\}, \quad (52)
\end{aligned}$$

where M_1 and M_2 denote complexity-accuracy tradeoff parameters, $\psi_{m_1}=\cos(\frac{2m_1-1}{2M_1}\pi)$, $q_{m_1}=\frac{\omega_4(1+\psi_{m_1})}{2\omega_3}$, $\psi_{m_2}=\cos(\frac{2m_2-1}{2M_2}\pi)$ and $q_{m_2}=\frac{(1+\psi_{m_2})\alpha_2}{2\alpha_1}+\frac{(1-\psi_{m_2})\omega_4}{2\omega_3}$. Following the same way, the EC of x_2 for $\frac{\omega_4}{\omega_3}\geq\frac{\alpha_2}{\alpha_1}$ can be written as

$$\begin{aligned}
&C_{x_2}^{\mathrm{SC}} = \frac{1}{4\ln 2}\\
&\times\int_0^{\frac{\alpha_2}{\alpha_1}}\frac{[1-\bar{F}_{\bar{Q}_3}(q)\bar{F}_{\bar{Q}_4}(q)][1-\bar{F}_{Q_1}(q)][1-\bar{F}_{Q_2}(q)]}{1+q}dq\\
&\approx\frac{\pi}{8\ln 2}\frac{\alpha_2}{\alpha_1}\sum_{n=1}^{N}\frac{\sqrt{1-\psi_n^2}}{N}\\
&\times\frac{[1-\bar{F}_{\bar{Q}_3}(q_n)\bar{F}_{\bar{Q}_4}(q_n)][1-\bar{F}_{Q_1}(q_n)][1-\bar{F}_{Q_2}(q_n)]}{1+q_n}, \quad (53)
\end{aligned}$$

where $\psi_n=\cos(\frac{2n-1}{2N}\pi)$, $q_n=\frac{\alpha_2(1+\psi_n)}{2\alpha_1}$, and N represents a complexity-accuracy tradeoff parameter.

Since $Q_4=\bar{Q}_3+\bar{Q}_4$, the CDF of Q_4 can be written as

$$F_{Q_4}(q_4)=\int_0^{\frac{\omega_4}{\omega_3}}\bar{F}_{\bar{Q}_4}(q_4-q)[\bar{F}_{\bar{Q}_3}(q)]'dq, \quad (54)$$

where $[\bar{F}_{\bar{Q}_3}(q)]' = -\frac{\omega_4}{a_1\rho_s(\omega_4-\omega_3 q)^2}\sum_{g_3=0}^{m_{12}-1}(\frac{m_{12}}{\Omega_{12}})^{g_3}/g_3!(g_3-\frac{m_{12}q}{\Omega_{12}a_1\rho_s(\omega_4-\omega_3 q)})(\frac{q}{a_1\rho_s(\omega_4-\omega_3 q)})^{g_3-1}e^{-\frac{m_{12}q}{\Omega_{12}a_1\rho_s(\omega_4-\omega_3 q)}}$. For mathematically intractable, we use Gaussian-Chebyshev quadrature to calculate (54) as

$$\begin{aligned}
F_{Q_4}(q_4)\approx&\frac{\omega_4\pi}{2\omega_3}\sum_{m_3=1}^{M_3}\frac{\sqrt{1-\psi_{m_3}^2}}{M_3}\\
&\times\bar{F}_{\bar{Q}_4}(q_4-q_{m_3})[\bar{F}_{\bar{Q}_3}(q_{m_3})]', \quad (55)
\end{aligned}$$

where $\psi_{m_3}=\cos(\frac{2m_3-1}{2M_3}\pi)$, $q_{m_3}=\frac{\omega_4(1+\psi_{m_3})}{2\omega_3}$, and M_3 is a complexity-accuracy tradeoff parameter. Thus, when MRC is adopted at U_2, we can use the order statistics and Gaussian-Chebyshev quadrature to obtain the EC of x_2 as

$$\begin{aligned}
C_{x_2}^{\mathrm{MRC}} &= \frac{1}{4\ln 2}\int_0^{\frac{\alpha_2}{\alpha_1}}\frac{[1-\bar{F}_{Q_1}(q)][1-\bar{F}_{Q_2}(q)][1-F_{Q_4}(q)]}{1+q}dq\\
&\approx\frac{\alpha_2\pi}{8\alpha_1\ln 2}\sum_{n_1=1}^{N_1}\frac{\sqrt{1-\psi_{n_1}^2}}{N_1}\\
&\times\frac{[1-\bar{F}_{Q_1}(q_{n_1})][1-\bar{F}_{Q_2}(q_{n_1})][1-F_{Q_4}(q_{n_1})]}{1+q_{n_1}}, \quad (56)
\end{aligned}$$

where $\psi_{n_1}=\cos(\frac{2n_1-1}{2N_1}\pi)$, $q_{n_1}=\frac{(1+\psi_{n_1})\alpha_2}{2\alpha_1}$, and N_1 is a complexity-accuracy tradeoff parameter. Combining (52), (53) and (56), we can obtain (27).

APPENDIX B
PROOF OF THEOREM 2

With imperfect SIC, the CDF of S_2 can be rewitten as

$$\begin{aligned}
F_{S_2}(s_2) =&1-\Delta_{l,l_1}{s_2}^{l}(s_2+D_3)^{-(l_1+m_{s1})}\\
&\times\exp\left(-\frac{m_{sr}s_2}{\omega_2 a_1\rho_s\Omega_{sr}}\right), \quad (57)
\end{aligned}$$

where $\Delta_{l,l_1}=\sum_{l=0}^{m_{sr}-1}\sum_{l_1=0}^{l}\binom{l}{l_1}\frac{{m_{s1}}^{m_{s1}}}{(\vartheta_2\Omega_{s1})^{m_{s1}}\Gamma(m_{s1})}(\frac{\omega_3}{\omega_2})^{-m_{s1}}\times\frac{(l_1+m_{s1}-1)!}{l!}(\omega_2 a_1\rho_s)^{l_1-l}(\frac{m_{sr}}{\Omega_{sr}})^{l-l_1-m_{s1}}$ and $D_3=\frac{\omega_2\Omega_{sr}m_{s1}}{m_{sr}\omega_3\vartheta_2\Omega_{s1}}$. Thus, using the order statistics and (22), we can calculate the EC of u_2 as

$$\begin{aligned}
C_{u_2} =&\frac{\Delta_{k,k_1}\Delta_{l,l_1}}{4\ln 2}\int_0^{\infty}(\bar{s}+D_1)^{-(k_1+m_{r1})}(\bar{s}+D_3)^{-(l_1+m_{s1})}\\
&\times(1+\bar{s})^{-1}\bar{s}^{k+l}\exp(-D_2\bar{s})d\bar{s}. \quad (58)
\end{aligned}$$

When $D_1\neq D_3$, through applying the partial fraction decomposition on $(\bar{s}+D_3)^{-(l_1+m_{s1})}(1+\bar{s})^{-1}$, we can rewrite (58) as

$$\begin{aligned}
C_{u_2} =&\frac{\Delta_{k,k_1}\Delta_{l,l_1}}{4\ln 2}\Bigg\{\sum_{\delta_1=1}^{l_1+m_{s1}}-(D_3-1)^{-\delta_1}\\
&\times\underbrace{\int_0^{\infty}(\bar{s}+D_1)^{-(k_1+m_{r1})}(\bar{s}+D_3)^{-\chi^*}\bar{s}^{k+l}\exp(-D_2\bar{s})d\bar{s}}_{\Xi_{11}}\\
&+(D_3-1)^{-(l_1+m_{s1})}\\
&\times\underbrace{\int_0^{\infty}(\bar{s}+D_1)^{-(k_1+m_{r1})}(1+\bar{s})^{-1}\bar{s}^{k+l}\exp(-D_2\bar{s})d\bar{s}}_{\Xi_{12}}\Bigg\}, \quad (59)
\end{aligned}$$

where $\chi^*=l_1+m_{s1}+1-\delta_1$.

Since $(\bar{s}+D_1)^{-(k_1+m_{r1})}(\bar{s}+D_3)^{-\chi^*}=\sum_{\chi_1=1}^{k_1+m_{r1}}\frac{d_{\chi_1}^1}{(\bar{s}+D_1)^{\chi_1}}+\sum_{\chi_2=1}^{\chi^*}\frac{d_{\chi_2}^2}{(\bar{s}+D_3)^{\chi_2}}$, $d_{\chi_1}^1=\frac{\partial^{k_1+m_{r1}-\chi_1}}{\partial\bar{s}^{k_1+m_{r1}-\chi_1}}[\frac{1}{(\bar{s}+D_3)^{\chi^*}}]|_{\bar{s}=-D_1}\times$

$\frac{1}{(k_1+m_{r1}-\chi_1)!}$ and $d^2_{\chi_2} = \frac{\partial^{\chi^*-\chi_2}}{\partial \bar{s}^{\chi^*-\chi_2}}[\frac{1}{(\bar{s}+D_1)^{k_1+m_{r1}}}]|_{\bar{s}=-D_3} \times \frac{1}{(\chi^*-\chi_2)!}$, we can use (26) to calculate Ξ_{11} as

$$\Xi_{11} = \sum_{\chi_1=1}^{k_1+m_{r1}} d^1_{\chi_1} I_2(k+l, D_1, \chi_1, D_2) + \sum_{\chi_2=1}^{\chi^*} d^2_{\chi_2} I_2(k+l, D_3, \chi_2, D_2). \quad (60)$$

Based on (36), we have $\Xi_{12} = \Xi$. Thus, substituting Ξ_{11} and Ξ_{12} into (59), we obtain C_{u_2} for $D_1 \neq D_3$.

When $D_1 = D_3$, implementing the partial fraction decomposition, (23) and (26) on (58), we have

$$\begin{aligned} C_{u_2} &= \frac{\Delta_{k,k_1}\Delta_{l,l_1}}{4\ln 2} \\ &\times \Bigg\{ \sum_{\delta_3=1}^{\delta^*} -(D_1-1)^{-\delta_3} \int_0^\infty (\bar{s}+D_1)^{-k^*} \bar{s}^{k+l} \exp(-D_2\bar{s}) d\bar{s} \\ &+ (D_1-1)^{-\delta^*} \int_0^\infty (1+\bar{s})^{-1} \bar{s}^{k+l} \exp(-D_2\bar{s}) d\bar{s} \Bigg\} \\ &= \frac{\Delta_{k,k_1}\Delta_{l,l_1}}{4\ln 2} \Bigg\{ \sum_{\delta_3=1}^{\delta^*} -(D_1-1)^{-\delta_3} I_2(k+l, D_1, k^*, D_2) \\ &+ (D_1-1)^{-\delta^*} I_1(k+l, D_2, \delta_4) \Bigg\}. \end{aligned} \quad (61)$$

Combining (58)-(61), we can obtain (37).

APPENDIX C
PROOF OF THEOREM 3

Applying the approximations of $\exp(z) \approx 1+z$ and $\mathrm{Ei}(-\mathrm{z}) \approx E^* + \ln(z) - z$ for $z \to 0$ to (21), we have

$$\begin{aligned} \tilde{C}^p_{x_1} \approx& -\frac{1}{4\ln 2} \Bigg\{ \Big(1+\frac{m_{s1}}{\alpha_1\rho_s\Omega_{s1}}\Big)\Big(E^* + \ln\Big(\frac{m_{s1}}{\alpha_1\rho_s\Omega_{s1}}\Big) \\ &- \frac{m_{s1}}{\alpha_1\rho_s\Omega_{s1}}\Big) - \sum_{\hat{b}=1}^{m_{s1}-1} (\hat{b}-1)!/\hat{b}! \Bigg\} \\ \approx& I_3\Big(m_{s1}, \frac{m_{s1}}{\alpha_1\rho_s\Omega_{s1}}, \hat{b}\Big), \end{aligned} \quad (62)$$

where $I_3(\cdot)$ has been defined in (40a).

Similarly, we approximate (31) and (32) as

$$\tilde{C}_{x_4} \approx I_3\Big(m_{r2}, \frac{m_{r2}}{a_2\rho_s\Omega_{r2}}, \hat{w}\Big), \quad (63)$$

$$\tilde{C}_{u_1} \approx I_3\Big(m_{s1}, \frac{m_{s1}}{\beta_1 a_1\rho_s\Omega_{s1}}, \hat{j}\Big). \quad (64)$$

When $\rho_s \to \infty$, $\gamma^{t_1}_{1,x_1} \approx \frac{\lambda_{s1}\alpha_1}{\lambda_{s1}\alpha_2}$ holds. Thus, we can apply [42, eq.(3.351.3)] to rewrite (24) as

$$F_P(p) \approx \hat{\Delta}_b p^b (A+p)^{-b-m_{s1}}, \quad (65)$$

where $\hat{\Delta}_b$ has defined in (43b). Furthermore, we can use [42, eq.(3.197.1)] to calculate $\tilde{C}_{x_1}$ as

$$\begin{aligned} \tilde{C}_{x_1} \approx& \frac{\hat{\Delta}_b}{4\ln 2} \int_0^\infty p^b (p+A)^{-b-m_{s1}} (1+p)^{-1} dp \\ \approx& \frac{\hat{\Delta}_b}{4\ln 2} A^{-b-m_{s1}} \mathcal{B}(b+1, m_{s1}) \\ &\times {}_2\mathcal{F}_1\Big(b+m_{s1}, b+1; b+m_{s1}+1, 1-\frac{1}{A}\Big) \\ \approx& \hat{\Delta}_b I_4(b, b+m_{s1}, 1, A, 1), \end{aligned} \quad (66)$$

where $I_4(\cdot)$ has been defined in (40b). Following the same steps in (65) and (66), we can obtain

$$\tilde{C}_{x_3} \approx \hat{\Delta}_i I_4(i, i+m_{r1}, 1, B, 1), \quad (67a)$$

$$\tilde{C}^p_{u_2} \approx \hat{\Delta}_k I_4(k, k+m_{r1}, 1, D_1, 1), \quad (67b)$$

$$\tilde{C}_{u_3} \approx \hat{\Delta}_v I_4(v, v+m_{sr}, 1, E, 1), \quad (67c)$$

where $\hat{\Delta}_i$, $\hat{\Delta}_v$ and $\hat{\Delta}_k$ have been defined in (43c), (43d) and (43e), respectively.

When the BS performs imperfect SIC, $\bar{S} \approx \{\frac{\lambda_{r2}\beta_2}{\lambda_{r1}\beta_1}, \frac{\lambda_{sr}\omega_2}{\lambda_{s1}\omega_3}\}$ holds. Thus, we can use [42, eq.(3.351.3)] and the order statistics to obtain the CDF of $\bar{S}$ for high SNR as

$$F_{\bar{S}}(\bar{s}) = 1 - \hat{\Delta}_k\hat{\Delta}_l \bar{s}^{k+l} (\bar{s}+D_1)^{-k-m_{r1}} (\bar{s}+D_3)^{-l-m_{s1}}, \quad (68)$$

where $\hat{\Delta}_l$ has been defined in (43f). Substituting (68) into (22), we have

$$\begin{aligned} \tilde{C}_{u_2} \approx& \frac{\hat{\Delta}_k\hat{\Delta}_l}{4\ln 2} \int_0^\infty (\bar{s}+D_1)^{-k-m_{r1}} (\bar{s}+D_3)^{-l-m_{s1}} \\ &\times \bar{s}^{k+l} (1+\bar{s})^{-1} d\bar{s}. \end{aligned} \quad (69)$$

When $D_1 \neq D_3$, through applying the partial fraction decomposition on $(\bar{s}+D_3)^{-(l_1+m_{s1})}(1+\bar{s})^{-1}$, we use [42, eq.(3.197.1)] to calculate (69) as

$$\begin{aligned} \tilde{C}_{u_2} \approx& \hat{\Delta}_k\hat{\Delta}_l \Bigg\{ \sum_{\delta_2=1}^{k+m_{r1}} -(D_1-1)^{-\delta_2} \\ &\times I_4(k+l, l+m_{s1}, \hat{k}, D_3, D_1) + (D_1-1)^{-(k+m_{r1})} \\ &\times I_4(k+l, l+m_{s1}, 1, D_3, 1) \Bigg\}. \end{aligned} \quad (70)$$

Conversely, if $D_1 = D_3$, we can directly use [42, eq.(3.197.1)] to obtain $\tilde{C}_{u_2}$ as

$$\tilde{C}_{u_2} \approx \hat{\Delta}_k\hat{\Delta}_l I_4(k+l, k+l+m_{r1}+m_{s1}, 1, D_1, 1). \quad (71)$$

Since $Q \approx \frac{\alpha_2}{\alpha_1}$ when $\rho_s \to \infty$. The asymptotic expression of x_2 can be given as

$$\tilde{C}_{x_2} \approx \frac{1}{4\ln 2} \ln\Big(\frac{\alpha_2}{\alpha_1}\Big). \quad (72)$$

Combining (62)-(72), we can obtain (41).

REFERENCES

[1] Z. Ding, X. Lei, G. K. Karagiannidis, R. Schober, J. Yuan, and V. Bhargava, "A survey on non-orthogonal multiple access for 5G networks: Research challenges and future trends," *IEEE J. Sel. Areas Commun.*, vol. 35, no. 10, pp. 2181–2195, Oct. 2017.

[2] T. N. Do, D. B. da Costa, T. Q. Duong, and B. An, "Improving the performance of cell-edge users in NOMA systems using cooperative relaying," *IEEE Trans. Commun.*, vol. 66, no. 5, pp. 1883–1901, May 2018.

[3] L. Dai, B. Wang, Z. Ding, Z. Wang, S. Chen, and L. Hanzo, "A survey of non-orthogonal multiple access for 5G," *IEEE Commun. Surveys Tuts.*, vol. 20, no. 3, pp. 2294–2323, 3rd Quart., 2018.

[4] Y. Liu, Z. Qin, M. Elkashlan, Z. Ding, A. Nallanathan, and L. Hanzo, "Nonorthogonal multiple access for 5G and beyond," *Proc. IEEE*, vol. 105, no. 12, pp. 2347–2381, Dec. 2017.

[5] Z. Yang, Z. Ding, P. Fan, and N. Al-Dhahir, "A general power allocation scheme to guarantee quality of service in downlink and uplink NOMA systems" *IEEE Trans. Wireless Commun.*, vol. 15, no. 11, pp. 7244–7257, Nov. 2016.

[6] P. D. Diamantoulakis, K. N. Pappi, Z. Ding, and G. K. Karagiannidis, "Wireless powered communications with non-orthogonal multiple access," *IEEE Trans. Wireless Commun.*, vol. 15, no. 12, pp. 8422–8436, Dec. 2016.

[7] Y. Xu, C. Shen, Z. Ding, X. Sun, S. Yan, G. Zhu, and Z. Zhong, "Joint beamforming and power-splitting control in downlink cooperative SWIPT NOMA systems," *IEEE Trans. Signal Process.*, vol. 65, no. 18, pp. 4874–4886, Sep. 2017.

[8] F. Zhou, Z. Chu, H. Sun, R. Q. Hu, and L. Hanzo, "Artificial noise aided secure cognitive beamforming for cooperative MISO-NOMA using SWIPT," *IEEE J. Sel. Areas Commun.*, vol. 36, no. 4, pp. 918–931, Apr. 2018.

[9] Z. Ding and H. V. Poor, "Design of massive-MIMO-NOMA with limited feedback," *IEEE Signal Process. Lett.*, vol. 23, no. 5, pp. 629–633, May 2016.

[10] W. M. Hao, M. Zeng, Z. Chu, and S. Yang, "Energy-efficient power allocation in millimeter wave massive MIMO with non-orthogonal multiple access," *IEEE Wireless Commun. Lett.*, vol. 6, no. 6, pp. 782–785, Dec. 2017.

[11] N. T. Do, D. B. da Costa, T. Q. Duong, and B. An, "A BNBF user selection scheme for NOMA-based cooperative relaying systems with SWIPT," *IEEE Commun. Lett.*, vol. 21, no. 3, pp. 664–667, Mar. 2017.

[12] N. Zhao, W. Wang, J. Wang, Y. Chen, Y. Lin, Z. Ding, and N. C. Beaulieu, "Joint beamforming and jamming optimization for secure transmission in MISO-NOMA networks," *IEEE Trans. Commun.*, vol. 67, no. 3, pp. 2294–2305, Mar. 2019.

[13] H. Lei, J. Zhang, K.-H. Park, P. Xu, I. S. Ansari, G. Pan, B. Alomair, and M. S. Alouini, "On secure NOMA systems with transmit antenna selection schemes," *IEEE Access*, vol. 5, pp. 17450–17464, Aug. 2017.

[14] B. Chen, Y. Chen, Y Cao, Y. Chen, N. Zhao, Z. Ding, and X. Wang, "Security enhancement using a novel two-slot cooperative NOMA scheme," *IEEE Trans. Veh. Technol.*, vol. 69, no. 3, pp. 3470-3475, Mar. 2020.

[15] Z. Ding, R. Schober, P. Fan, and H. Vincent Poor, "OTFS-NOMA: An efficient approach for exploiting heterogenous user mobility profiles," *IEEE Trans. Commun.*, vol. 67, no. 11, pp. 7950–7965, Nov. 2019.

[16] Z. Ding and H. V. Poor, "A simple design of IRS-NOMA transmission," *IEEE Commun. Lett.*, vol. 24, no. 5, pp. 1119-1123, May 2020.

[17] Z. Ding, M. Peng, and H. V. Poor, "Cooperative non-orthogonal multiple access in 5G systems," *IEEE Commun. Lett.*, vol. 19, no. 8, pp. 1462–1465, Aug. 2015.

[18] J. Men, J. Ge, and C. Zhang, "Performance analysis of nonorthogonal multiple access for relaying networks over Nakagami-m fading channels," *IEEE Trans. Veh. Technol.*, vol. 66, no. 2, pp. 1200–1208, Feb. 2017.

[19] L. Lv, Q. Ni, Z. Ding, and J. Chen, "Application of non-orthogonal multiple access in cooperative spectrum-sharing networks over Nakagami-m fading channels," *IEEE Trans. Veh. Technol.*, vol. 66, no. 6, pp. 5506–5511, Jun. 2017.

[20] W. Mei and R. Zhang, "Uplink cooperative NOMA for cellular-connected UAV," *IEEE J. Sel. Areas Commun.*, vol. 13, no. 3, pp. 644–656, Jun. 2019.

[21] L. Zhang, J. Liu, M. Xiao, G. Wu, Y. C. Liang, and S. Li, "Performance analysis and optimization in downlink NOMA systems with cooperative full-duplex relaying," *IEEE J. Sel. Areas Commun.*, vol. 35, no. 10, pp. 2398–2412, Oct. 2017.

[22] C. Dai, T. Thai, and P. Popovski, "Coordinated direct and relay transmission with interference cancelation in wireless systems," *IEEE Commun. Lett.*, vol. 15, no. 4, pp. 416-418, Apr. 2011.

[23] J.-B. Kim and I.-H. Lee, "Non-orthogonal multiple access in coordinated direct and relay transmission," *IEEE Commun. Lett.*, vol. 19, no. 11, pp. 2037–2040, Nov. 2015.

[24] C. Zhong and Z. Zhang, "Non-orthogonal multiple access with cooperative full-duplex relaying," *IEEE Commun. Lett.*, vol. 20, no. 12, pp. 2478–2481, Dec. 2016.

[25] V. Aswathi and A. V. Babu, "Full/half duplex cooperative NOMA under imperfect successive interference cancellation and channel state estimation errors," *IEEE Access*, vol. 7, pp. 179961-179984, Dec. 2019.

[26] H. Liu, Z. Ding, K. J. Kim, K. S. Kwak, and H. V. Poor, "Decode-and-forward relaying for cooperative NOMA systems with direct links," *IEEE Trans. Wireless. Commun.*, vol. 17, no. 12, pp. 8077–8093, Dec. 2018.

[27] M. F. Kader and S. Y. Shin, "Coordinated direct and relay transmission using uplink NOMA," *IEEE Wireless Commun. Lett.*, vol. 7, no. 8, pp. 400–403, Jun. 2018.

[28] Y. Xu, G. Wang, L. Zheng, and S. Jia, "Performance of NOMA-based coordinated direct and relay transmission using dynamic scheme," *IET Commun.*, vol. 12, no. 18, pp. 2231–2242, Nov. 2018.

[29] M. Yang, J. Chen, L. Yang, L. Lv, B. He, and B. Liu, "Design and performance analysis of cooperative NOMA with coordinated direct and relay transmission," *IEEE Access*, vol. 7, pp. 73306–73323, Jun. 2019.

[30] J.-B. Kim, I.-H. Lee, and J. Lee, "Capacity scaling for D2D aided cooperative relaying systems using NOMA," *IEEE Commun. Lett.*, vol. 7, no. 1, pp. 42–45, Feb. 2018.

[31] L. Zou, J. Chen, L. Lv, and B. He, "Capacity enhancement of D2D aided coordinated direct and relay transmission using NOMA," *IEEE Commun. Lett.*, to appear.

[32] X. Li, Y. Chen, P. Xue, G. Lv, and M. Shu, "Outage performance for satellite-assisted cooperative NOMA systems with coordinated direct and relay transmission," *IEEE Commun. Lett.*, to appear.

[33] Y. Cao, N. Zhao, G. Pan, Y. Chen, L. Fan, M. Jin, and M.-S. Alouini, "Secrecy analysis for cooperative NOMA networks with multi-antenna full-duplex relay," *IEEE Trans. Commun.*, vol. 67, no. 8, pp. 5574–5587, Aug. 2019.

[34] Y. Guo, Y. Li, Y. Li, W. Cheng, and H. Zhang, "SWIPT assisted NOMA for coordinated direct and relay transmission," in *Proc. IEEE/CIC Int. Conf. Commun. China (ICCC)*, Beijing, China, Aug. 2018, pp. 111–115.

[35] X. Chen, G. Liu, Z. Ma, X. Zhang, W. Xu, and P. Fan, "Optimal power allocations for non-orthogonal multiple access over 5G full/half-duplex relaying mobile wireless networks," *IEEE Trans. Wireless Commun.*, vol. 18, no. 1, pp. 77–92, Jan. 2019.

[36] C. Li and X. Li, "Throughput maximization for multi-carrier non-orthogonal multiple access systems with coordinated direct and relay transmission," in *Proc. IEEE Int. Conf. Commun. (ICC)*, Kansas City, MO, USA, May 2018, pp. 1-6.

[37] D. Tse and P. Viswanath, *Fundamentals Wireless Communication.* Cambridge, U.K.: Cambridge Univ. Press, 2005.

[38] L. Lv, H. Jiang, Z. Ding, L. Yang, and J. Chen, "Secrecy-enhancing design for cooperative downlink and uplink NOMA with an untrusted relay," *IEEE Trans. Commun.*, vol. 68, no. 3, pp. 1698-1715, Mar. 2020.

[39] K. Reshma and A. V. Babu, "Throughput analysis of energy harvesting enabled incremental relaying NOMA system," *IEEE Commun. Lett.*, vol. 24, no. 7, pp. 1419-1423, Jul. 2020.

[40] S. Abeywickrama, L. Liu, Y. Chi, and C. Yuen, "Over-the-air implementation of uplink NOMA," in *Proc. IEEE Glob. Commun. Conf.*, Dec. 2017, pp. 1-6.

[41] Y. Liu, Z. Ding, M. Elkashlan, and H. V. Poor, "Cooperative nonorthogonal multiple access with simultaneous wireless information and power transfer," *IEEE J. Sel. Areas Commun.*, vol. 34, no. 4, pp. 938-953, Apr. 2016.

[42] I. S. Gradshteyn and I. M. Ryzhik, *Tables of Integrals, Series, and Products*, 7th ed. New York, NY, USA: Academic, 2007.

[43] Zheng, X. Wang, M. Wen, and F.-J. Chen, "NOMA-based multi-pair two-way relay networks with rate splitting and group decoding," *IEEE J. Sel. Areas Commun.*, vol. 35, no. 10, pp. 2328-2341, Oct. 2017.

[44] D. Nguyen, L.-N. Tran, P. Pirinen, and M. Latva-Aho, "Precoding for full duplex multiuser MIMO systems: Spectral and energy efficiency maximization," *IEEE Trans. Signal Process.*, vol. 61, no. 16, pp. 4038-4050, Aug. 2013.

[45] J. Bae and Y. Han, "Joint power and time allocation for two-way cooperative NOMA," *IEEE Trans. Veh. Technol.*, vol. 68, no. 12, pp. 12443-12447, Dec. 2019.

[46] A. Sediq, R. Gohary, R. Schoenen, and H. Yanikomeroglu, "Optimal tradeoff between sum-rate efficiency and Jain's fairness index in resource allocation," *IEEE Trans. Wireless Commun.*, vol. 12, no. 7, pp. 3496-3509, Jul. 2013.
[47] F. Fang, H. Zhang, J. Cheng, and V. C. M. Leung, "Energy-efficient resource allocation for downlink non-orthogonal multiple access network," *IEEE Trans. Commun.*, vol. 64, no. 9, pp. 3722-3732, Sep. 2016.
[48] C. Zhong, K. Wong, and S. Jin, "Capacity bounds for MIMO Nakagami-m fading channels," *IEEE Trans. Signal Process.*, vol. 57, no. 9, pp. 3613-3623, Sep. 2009.
[49] D. Wan, M. Wen, F. Ji, Y. Liu, and Y. Huang, "Cooperative NOMA systems with partial channel state information over Nakagami-m fading channels," *IEEE Trans. Commun.*, vol. 66, no. 3, pp. 947-958, Mar. 2018.